Optics Communications 406 (2018) 214–229

Contents lists available at ScienceDirect

Optics Communications

journal homepage: www.elsevier.com/locate/optcom

High-performance mode-locked and Q-switched fiber lasers based on novel 2D materials of topological insulators, transition metal dichalcogenides and black phosphorus: review and perspective (invited)

Kan Wu [a,*], Bohua Chen [a], Xiaoyan Zhang [b], Saifeng Zhang [b], Chaoshi Guo [a], Chao Li [a], Pushan Xiao [a], Jun Wang [b], Linjie Zhou [a], Weiwen Zou [a], Jianping Chen [a,*]

[a] State Key Laboratory of Advanced Optical Communication Systems and Networks, Department of Electronic Engineering, Shanghai Jiao Tong University, Shanghai 200240, China

[b] Key Laboratory of Materials for High-Power Laser, Shanghai Institute of Optics and Fine Mechanics, Chinese Academy of Sciences, Shanghai 201800, China

ARTICLE INFO

Keywords:
Mode lock, Q-switch
2D material
Topological insulator
Transition metal dichalcogenides
Black phosphorus

ABSTRACT

The discovery of two-dimensional (2D) material graphene has opened a door towards a class of layered novel nanomaterials with unique photonic and optoelectronic properties. Recently many new 2D materials have been reported, including topological insulators (TIs), transition metal dichalcogenides (TMDs) and black phosphorus (BP). These materials have been demonstrated high optical nonlinearity and Pauli blocking used as saturable absorbers (SAs) in pulsed lasers. In this paper, we summarize the current specifications from these 2D materials based mode-locked and Q-switched lasers. The laser performance in operating wavelength, optical bandwidth, repetition rate and pulse energy is reviewed. Finally future perspective is suggested.

1. Introduction

The discovery of graphene has opened a door towards novel two-dimensional (2D) materials with unique photonic and optoelectronic properties. Many different photonic devices have been demonstrated with 2D materials including optical modulator, photodetector, saturable absorber, and optical switch. Among various 2D materials after graphene, there are three widely investigated types, i.e., topological insulators (TIs), layered transition metal dichalcogenides (TMDs) and recently discovered black phosphorus (BP, also known as phosphorene). It now has been recognized that 2D materials may share many similar photonic properties such as wide range of linear optical absorption, Pauli blocking induced saturable absorption as well as ultrafast relaxation time, and high optical nonlinearity. Therefore, investigation on one type of 2D materials may benefit the research on other 2D materials. Meanwhile, pulsed laser is an important technology covering from fundamental scientific research to practical industrial application. Many 2D materials have been reported saturable absorption and utilized in lasers to trigger pulsed operation.

In this paper, we review the mode-locked and Q-switched lasers based on three typical 2D materials TIs, TMDs and BP. The material fabrication and characterization are briefly introduced to give a complete picture of these 2D materials. Then the mode-locked and Q-switched lasers based on these three materials are summarized. The extremity of laser specifications is paid special attention, including operating wavelength, optical bandwidth, repetition rate and pulse energy. Finally conclusions are made and future perspective is suggested.

2. Material fabrication and characterization

Here we focus on three 2D materials TIs, TMDs and BP because they are most widely used in mode-locked and Q-switched lasers after graphene. Before the discussion on their fabrication and characterization methods, we first briefly introduce these three 2D materials.

Topological insulators are a series of Dirac materials resembling graphene. There are tens of detailed compounds which have been identified such as Bi_2Te_3, Bi_2Se_3 and Sb_2Te_3. They have insulating bandgaps in bulk but gapless surface states with a linear dispersion relation between energy and momentum of surficial Dirac electrons originating from strong spin-orbit coupling. This leads to a wideband absorption of optical photons and TIs can be used as saturable absorbers (SAs) in pulsed lasers. The first demonstration of SA behavior of TIs was a Bi_2Te_3 based mode-locked fiber laser near 1550 nm in 2012 [1,2]. Ever

* Corresponding authors.
E-mail addresses: kanwu@sjtu.edu.cn (K. Wu), jpchen62@sjtu.edu.cn (J. Chen).

http://dx.doi.org/10.1016/j.optcom.2017.02.024
Received 28 December 2016; Received in revised form 8 February 2017; Accepted 10 February 2017
Available online 21 February 2017
0030-4018/

since that discovery, other TI materials have been deployed in mode-locked lasers with different operating wavelengths [2–4]. Besides mode-locked lasers, Q-switched lasers based on TIs have also been intensively reported [5–7].

TMDs are a cluster of compounds with a general chemical formula MX_2 where M stands for transition metal element from IVB-VIIB in periodic table of elements and X is chalcogen. Typical TMDs include MoS_2, WS_2, $MoSe_2$ and WSe_2. In bulk state, they are semiconductors with indirect bandgap. However, when exfoliated to monolayer, they exhibit direct bandgap. Experiments have demonstrated the bandgap tunability by altering layer numbers or introducing defects which is beneficial to find applications in optoelectronics [8]. Few-layer TMDs materials had been verified to exhibit a wideband optical saturable absorption. In 2013, Wang et al. have firstly observed saturable absorption of MoS_2 [9].

Different from semi-metallic graphene and semiconductor transition metal dichalcogenides, BP, also called phosphorene to follow the naming of graphene, is a direct bandgap semiconductor from monolayer to few layers which allows to control bandgap by altering number of layers. Under strong illumination of optical light, BP can be saturated which means it could be acted as saturable absorber for pulsed lasers [10]. The first demonstration of a BP based mode-locked and Q-switched fiber laser near 1550 nm was reported in 2015 [11].

2.1. Fabrication method

The fabrication methods of 2D materials can be generally classified into 2 main categories: top-down methods which exfoliate bulk materials down to mono- or few-layer 2D nanosheets by breaking the van der Waals force between layers, and bottom-up methods which synthesize nanomaterials directly on molecular level. A few developed fabrication methods are summarized in Fig. 1. Among these methods, some are purely physical without chemical reactions involved in the fabrication such as mechanical exfoliation (ME) and liquid-phase exfoliation (LPE), while others are chemical such as Lithium ion intercalation exfoliation and chemical vapor deposition (CVD). Here we will briefly introduce three methods among them which are widely used for laser applications. They are mechanical exfoliation, solution processing (including Lithium ion intercalation exfoliation and liquid-phase exfoliation) and chemical vapor deposition.

2.1.1. Mechanical exfoliation

Assisting by van der Waals force, many layers of 2D monolayer materials gather together to form bulk materials. Reversely, breaking apart layers from bulk materials by overcoming this force allows researchers to obtain high quality 2D mono- and few-layer materials. Mechanical exfoliation is such a method which adopts scotch tapes to peel and take apart bulk materials repeatedly until obtaining mono- or few-layer materials. It was firstly used in discovering graphene from graphite flakes by Geim and Novoselov in 2004 [12]. This method is easy to carry out. The exfoliated mono- or few-layer materials have high completeness and less defects suitable for fundamental scientific research. It can also been used to obtain other 2D materials such as topological insulators [13–15]. However, yield of this method is very low and repeated operation is required.

2.1.2. Solution processing

Solution processing takes advantage of interaction between specific solvents and bulk materials to exfoliate into mono- or few-layer materials under solution environment. The surface energy of the solvent molecules is chosen to be close to that of 2D nanomaterials so that the material nanosheets can exist stably without re-aggregation when they are exfoliated from bulk materials physically or chemically. Commonly used solvents are NMP (N-methyl-2-pyrrolidone) [7,16,17], acetone [18–20], IPA (isopropyl alcohol) [5,6,21], DMF (dimethyl formamide) [9,22], and ethanol [23–25] as well as surfactant sodium cholate [26–28]. Some researchers also explore other solvents such as chitosan [4]. Lithium ion intercalation exfoliation is a typical chemical exfoliation method which uses lithium ions as intercalant to widen layer separation in bulk materials and then applying mechanical force by stirring or ultra-sonication to dissociate 2D materials [29,30]. This method can afford high-yield production of 2D material nanosheets. However, produced nanomaterials usually have deficiency such as structure alteration and post-processing is sometimes required to improve the quality. Another prevalent mean is liquid-phase exfoliation which is a purely physical method. LPE directly uses high-strength ultra-sonication to generate micro bubbles and forces in the materials to break the van der Waals force between layers. After sonication, centrifugation is applied to separate residual un-exfoliated material flakes and layered 2D nanosheets. Un-exfoliated flakes will fall down to the bottom in

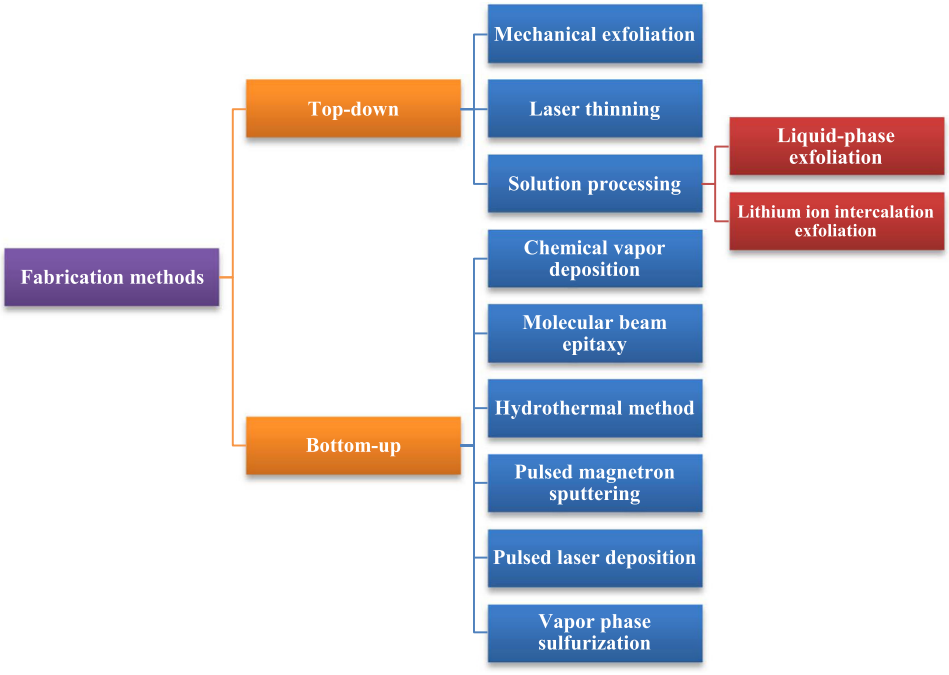

Fig. 1. Classification of fabrication methods of 2D materials.

the dispersions and the 2D nanosheets suspended on the top can be collected. By adjusting the time and strength of ultra-sonication and centrifugation process, the number of layers of exfoliated nanosheets can be roughly controlled. LPE provides a facile and low-cost method to produce large amounts of mono- and few-layer 2D materials and no post-processing is required compared with chemical solution processing method. Monolayer nanosheets can be generated by LPE but the concentration compared with few-layer nanosheets is usually low.

2.1.3. Chemical vapor deposition

Chemical vapor deposition is an important and scalable method to synthesize large-scale 2D materials. Typically, gaseous or powder reactants are fed into reaction chamber and 2D materials can be produced from specific chemical reaction under appropriate conditions. By placing certain substrate in the reaction chamber, 2D materials can directly grow on the substrate. Compared with solution processing method, the number of layers of 2D materials produced by CVD can be controlled with good accuracy by modifying reaction parameters [31]. High yields make this method a main method to synthesize commercially available 2D materials. However, cost and process complexity might be high.

The following table compares the abovementioned three methods on a few specifications. It can be seen that different methods have their own pros and cons and should be chosen based on the requirement of specific applications. (Table 1).

2.1.4. Other methods

There are other fabrication methods put forward by researchers for specific 2D nanomaterials. Molecular beam epitaxy (MBE) can grow high quality topological insulator film on bulk substrates while the disadvantage lies in requirement for expensive equipment [32]. Pulsed magnetron-sputtering technology has also been deployed in fabricating topological insulator nanomaterials [33,34]. Pulsed laser deposition employs pulsed laser as ablation source to evaporate material in a vacuum chamber and then molecules deposit on the surface of suitable substrate [35,36]. Hydrothermal method crystallizes nano flakes by hydrothermal reaction between reactants and can be used to fabricate TMDs [37]. Vapor phase sulfurization makes use of sulfur vapor to sulfurize thin metal films such as W, Mo under high temperature and synthesize few-layer TMDs [38]. Laser thinning method sublimates upper layers of solid bulk material with heat induced by light absorption and leaves single bottom layer on the substrate [39].

2.2. Material characterization

Material characterization applies suitable detection methods to evaluate the quality or characteristics of a certain material. 2D materials can be evaluated from several aspects including number of layers, dimension of nanosheets, absorption spectrum and so on. Every trait can be assessed by specific test equipment and corresponding methods. Here several principal characterization means are enumerated, shown in Fig. 2.

Transmission electron microscopy (TEM) is utilized to measure dimensional information such as width and length of the material nanosheets. TEM can also partially indicate layer information by comparing different colors of the nanosheets. Atomic force microscopy (AFM) is adopted to characterize the thickness of fabricated nanomaterials. By using a probe (a tip) to scan the surface of the nanomaterials, AFM can reveal the surface morphology of the sample. AFM is one of the most accurate methods to estimate the number of layers of a certain nanomaterial because the relation between the thickness and number of layers of a certain nanomaterial can be theoretically calculated. For example, monolayer MoS_2 is ~0.65 nm [40], monolayer WS_2 is ~0.9 nm [41] and monolayer BP (phosphorene) is ~0.6 nm [42]. Raman spectroscopy is a powerful tool to determine the molecular structures of the materials. Stimulated by laser with suitable intensity, molecular structures vibrating in a certain mode absorb the corresponding energy from the incident photons and emit new photons with lower energy. The energy difference (or frequency shift) between the incident photons and newly emitted photons indicate the information of molecular structures. Different vibration modes correspond to different frequency shift. For some 2D materials such as MoS_2 and WS_2, the distance between two certain peaks on the Raman spectrum is also related to the layered structure and thus can be used to estimate the number of layers [43]. The Raman spectrum may also depend on the polarization of the incident light and thus can be used to estimate the crystalline orientation of the nanomaterials [44]. Another tool to investigate band structures of 2D materials is linear transmission (or absorption) measurement which provides information about absorption spectrum. For a certain nanomaterial, different number of layers and different composition correspond to different band structures and result in different absorption peaks in the spectrum. Therefore observation of certain absorption peaks in the sample reveals the existence of 2D materials with certain number of layers or components. There is also nonlinear transmission (or absorption) measurement which will be discussed in the following section.

Table 1
Comparison of three typical fabrication methods.

Methods	Quality	Monolayer fab.	Yields/ round	Process complexity	Cost
Mechanical exfoliation	High	Yes	Low	High	Low
Solution processing	Medium	Yes, but mixed with few-layer ones	High	Medium	Low
Chemical vapor deposition	High	Yes	High	High	High

2.3. Optical nonlinearity – Kerr effect and saturable absorption

Optical nonlinearity plays an important role in many photonic and optoelectronic applications. When the intensity of incident light is low, the response of materials is linear, that is, the amplitude, phase, polarization or other properties of the light may be modified, but no new frequency component will be generated. In contrast, nonlinear response of materials occurs when the light intensity is high. There are many origins of optical nonlinearity. Some have energy exchange between light and materials (inelastic nonlinearity) and some others don't (elastic nonlinearity). In this part, we describe two well-known nonlinear effects in 2D materials, they are Kerr effect and saturable absorption.

Kerr effect is a typical elastic nonlinear effect, i.e., there is no energy exchange between light and materials. Fundamentally, Kerr effect is related to the aharmonic motion of electrons under highly intense electromagnetic field of the light [45]. A total polarization **P** is used to model linear and nonlinear responses under electrical field **E**, given by [45].

$$\mathbf{P} = \varepsilon_0(\chi^{(1)} \cdot \mathbf{E} + \chi^{(2)} : \mathbf{E} + \chi^{(3)} \vdots \mathbf{EEE} + \ldots) \quad (1)$$

where ε_0 is the vacuum permittivity. First-order susceptibility $\chi^{(1)}$ represents the linear response of the material. Second-order susceptibility $\chi^{(2)}$ represents two-frequency effects such as second harmonic generation and sum-frequency generation. It is non-zero only when there is no inversion symmetry in the material molecules. Third-order susceptibility $\chi^{(3)}$ represents three-frequency effects such as four-wave mixing and third harmonic generation. The real part of third-order susceptibility $\chi^{(3)}$ represents the nonlinear phase change of incident light field induced by the materials, known as Kerr effect. The total energy of the incident light is unchanged in Kerr effect. In fiber optics, another nonlinear parameter n_2 is more commonly used to depict Kerr

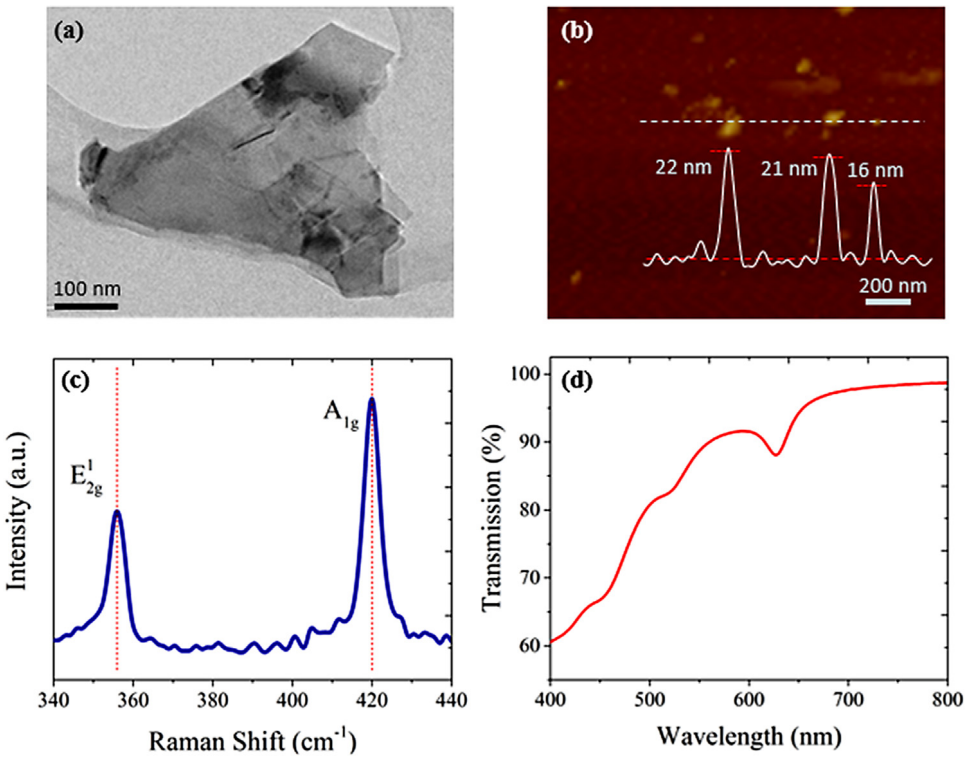

Fig. 2. Examples of typical characterization methods of 2D materials, (a) transmission electron microscopy image of MoS_2 [26], (b) atomic force microscopy image of MoS_2, (c) Raman spectrum of WS_2 [26], (d) linear transmission spectrum of WS_2 ([26] used with permission of OSA).

effect. The refractive index n under high optical intensity I is given by [45].

$$n = n_0 + n_2 I \tag{2}$$

where n_0 is the linear refractive index. The nonlinear refractive index coefficient n_2 is related to the real part of $\chi^{(3)}$, given by [46,47].

$$\mathrm{Re}\chi^{(3)}_{monolayer} = \frac{{n_0}^2 n_2 (cm^2/W)}{0.0395 N^2_{eff}} \tag{3}$$

where $\chi^{(3)}_{monolayer}$ is the susceptibility of monolayer materials, N_{eff} is the effective number of layer. Total susceptibility is given by $\chi^{(3)}_{total} = N^2_{eff}\chi^{(3)}_{monolayer}$. Different from Kerr effect, saturable absorption is an inelastic nonlinear effect, i.e., there is energy exchange between light and materials. The imaginary part of $\chi^{(3)}$ represents the nonlinear absorption of the materials under incident light field. Saturable absorption is one kind of nonlinear absorption and is related to the imaginary part of $\chi^{(3)}$. But there are also other kinds of nonlinear absorption such as two-photon absorption (TPA) and free-carrier absorption (FCA) in semiconductor. Many effects can result in saturable absorption. For 2D materials, the origin of saturable absorption is usually believed to be Pauli blocking [48]. When a light beam shines on a 2D material, electrons in the valence band are excited to the conduction band. Then these electrons gradually lose their energy due to various scattering effects and fall down to a lower position in the conduction band. When there are many electrons excited in the same time by a highly intense light beam, the conduction band will be completely filled with electrons and no more photons will be absorbed. In this case, the absorption of the material is reduced and the material is known as "saturated" or "bleached". Such a material is called a saturable absorber. The word "bleached" is used because early saturable absorbers are mostly dyes.

The absorption coefficient α of a saturable absorber is modelled by [48]

$$\alpha = \alpha_{ns} + \frac{\alpha_s}{1 + I/I_{sat}} \tag{4}$$

where α_{ns} is the non-saturable absorption coefficient representing the intensity independent loss, α_s is saturable absorption coefficient, I is the incident optical intensity and I_{sat} is the saturation intensity. When the light intensity is low, the absorption is equal to $\alpha_{ns}+\alpha_s$ and when the intensity is high, the absorption is equal to α_{ns}. The maximum change of the absorption is α_s. Two photon absorption is also a nonlinear absorption effect in the materials which means the electrons absorb two photons simultaneously to be excited to the conduction band. When the light intensity is very high, TPA becomes significant enough and should be taken into consideration. The saturable absorption expression including TPA effect is given by [9]

$$\alpha = \alpha_{ns} + \frac{\alpha_s}{1 + I/I_{sat}} + \beta I \tag{5}$$

where β is the TPA coefficient. The transmission T is then given by

$$\begin{aligned} T &= \exp(-\alpha) = \exp\left(-\alpha_{ns} - \frac{\alpha_s}{1 + I/I_{sat}} - \beta I\right) \\ &\approx \exp(-\alpha_{ns})\left(1 - \frac{\alpha_s}{1 + I/I_{sat}} - \beta I\right) = T_0 - \frac{T_0 \alpha_s}{1 + I/I_{sat}} - T_0 \beta I \end{aligned} \tag{6}$$

where we assume α_s and βI are much smaller than 1 and low-intensity transmission $T_0 = \exp(-\alpha_{ns})$. The absorption coefficient α is often normalized to the material thickness L to eliminate the influence of different sample thickness, i.e., the normalized absorption coefficient $\alpha_0 = \alpha/L$. There is also another absorption parameter called absorbance A. It is related to the transmission T by $T = 10^{-A}$. The relation between absorption coefficient α and absorbance A is given by $A = \lg e \cdot \alpha = 0.434\alpha$. The absorbance A can also be normalized to the material thickness L to define the normalized absorbance $A_0 = A/L$. Absorption coefficient α, absorbance A and transmission T are all unitless while normalized absorption coefficient α_0 and absorbance A_0 have the units of m^{-1}.

Sometimes the model in Eqs.(4)–(6) does not work well with the measured data because the term $(1 + I/I_{sat})^{-1}$ requires a wide transition region to change from unsaturated (e.g., $I = 0.1I_{sat}$) to saturated state (e.g., $I = 10I_{sat}$). That is, the incident intensity I needs to be increased by 100 times to saturate the SA. In many reported saturable absorption

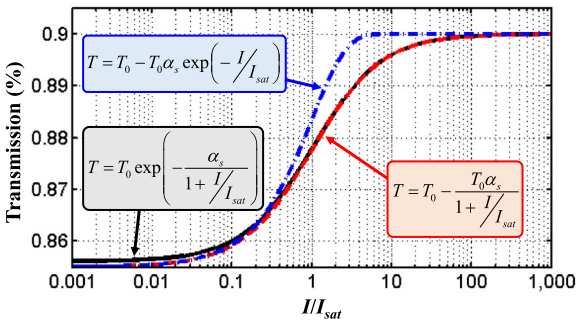

Fig. 3. Comparison of different SA models where $T_0 = 0.9$ and $\alpha_s = 0.05$.

measurement, the transition region is narrower than the model. Therefore, a modified model is also widely used, given by Eq.(7) [49] and a comparison of different SA models are shown in Fig. 3.

$$T = T_0 - \Delta T \exp(-I/I_{sat}) - T_0 \beta I \tag{7}$$

For 2D materials, two measurement methods are generally used to characterize the Kerr effect and saturable absorption, they are Z-scan measurement and two-arm measurement. A typical Z-scan measurement setup is shown in Fig. 4(a). The sample is mounted on a Z-direction translation stage. The light from a pulsed source (can be nanosecond, picosecond or femtosecond pulses) is first split to two paths. One path with low optical power is for reference and is measured by a slow detector (powermeter). The other path with high optical power is for material characterization. The light beam in the measurement path is then focused to the sample by a lens. The transmitted light beam after the sample is collected by a second detector. If there is an aperture before the second detector, the Z-scan measurement is called closed-aperture. Otherwise the Z-scan is called open-aperture. In the measurement, the translation stage is moved along the light beam so that the sample will experience different light intensity due to the different beam size. For open-aperture Z-scan measurement, the intensity dependent transmission of the sample can be obtained by comparing the readings of two detectors. Open-aperture Z-scan measurement is therefore able to measure the saturable absorption of the sample. For closed-aperture Z-scan measurement, the reading from the second detector is not only dependent on the transmission of the sample but also the beam diameter after the sample. Because the beam diameter after the sample is related to the beam induced refractive index change of the sample, closed-aperture Z-scan measurement is able to investigate the Kerr effect of the sample and obtain the real part of third-order susceptibility $\chi^{(3)}$ and nonlinear index parameter n_2. More details on the mathematical analysis of Z-scan measurement can be referred to Ref.[50]. Fig. 4(b) shows typical results in open-aperture and closed-aperture Z-scan measurement. Position (intensity) dependent transmission can be clearly observed. Fig. 4(c) shows a typical spatial pattern when a light beam propagates through 2D material dispersions and the beam deformation with ring pattern is observed. Many 2D materials have been characterized its third-order susceptibility $\chi^{(3)}$ and other related parameters. For example, the typical values for TMD nanosheets dispersions are $3{\cdot}10^{-9} \sim 7.75{\cdot}10^{-9}$ esu for $\mathrm{Re}\chi^{(3)}$ and $9.32{\cdot}10^{-7} \sim 6.49{\cdot}10^{-7}$ cm^2/W for n_2. For TMD thin films, the typical values are $-1.26{\cdot}10^{-10} \sim 4.82{\cdot}10^{-9}$ esu for $\mathrm{Re}\chi^{(3)}$ and $-3.36{\cdot}10^{-12} \sim 1.28{\cdot}10^{-10}$ cm^2/W for n_2, $4.2{\cdot}10^{-10} \sim 4{\cdot}10^{-8}$ esu for $\mathrm{Im}\chi^{(3)}$. For TI Bi_2Te_3 dispersions, the typical values are 10^{-7} esu for $\mathrm{Re}\chi^{(3)}$ and $2.11{\cdot}10^{-8}$ cm^2/W for n_2. For BP dispersions, the typical values are $2.56 \sim 4.18{\cdot}10^{-8}$ esu for $\mathrm{Re}\chi^{(3)}$ and $2.27 \sim 3.71{\cdot}10^{-5}$ cm^2/W for n_2. More detailed information and data can be referred to Ref. [38,46,51–53].

Two-arm measurement is the fiber version of open-aperture Z-scan measurement. Its setup is shown in Fig. 5(a). All the light propagation is confined in optical fiber. The light beam from a pulsed laser source (usually a femtosecond laser) propagates through a variable attenuator and is then split by a fiber coupler. The small portion of the power is measured by a slow detector (powermeter) for reference. The large portion of the power is injected into the sample and then measured by a second detector. Different from open-aperture Z-scan setup, the sample is incorporated to fiber (e.g., embedded between two fiber connectors or deposited on side-polished fiber) and there is no translation stage. Instead the power from the light source is adjusted by the variable attenuator to change the light intensity shining on the sample. Because

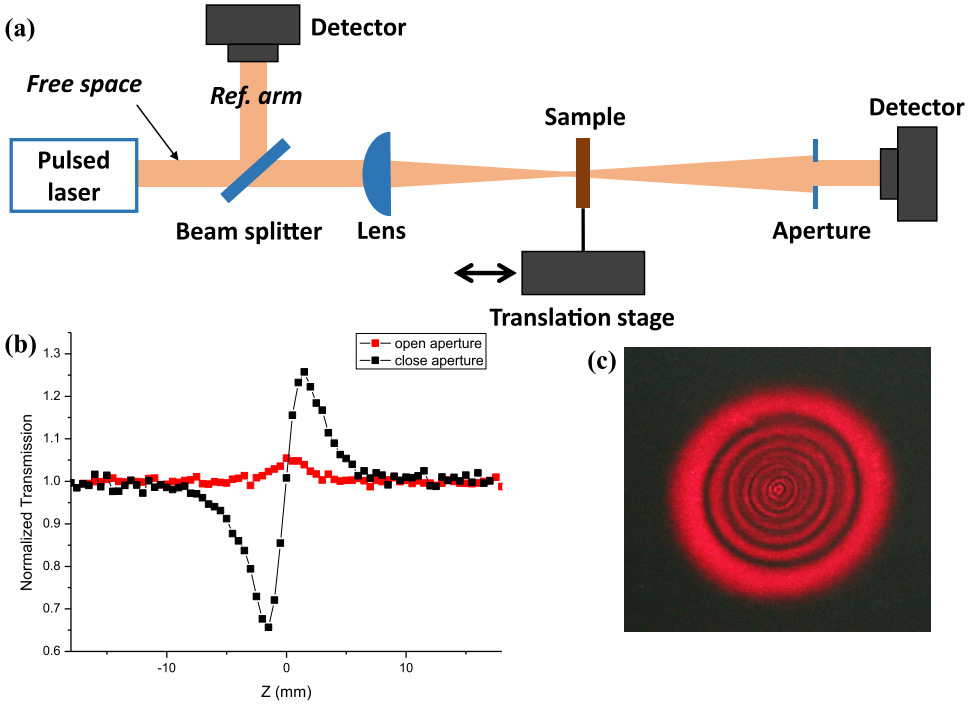

Fig. 4. (a) Z-scan measurement setup, (b) typical Z-scan measurement results, and (c) beam with ring pattern induced by nonlinear refractive index change.

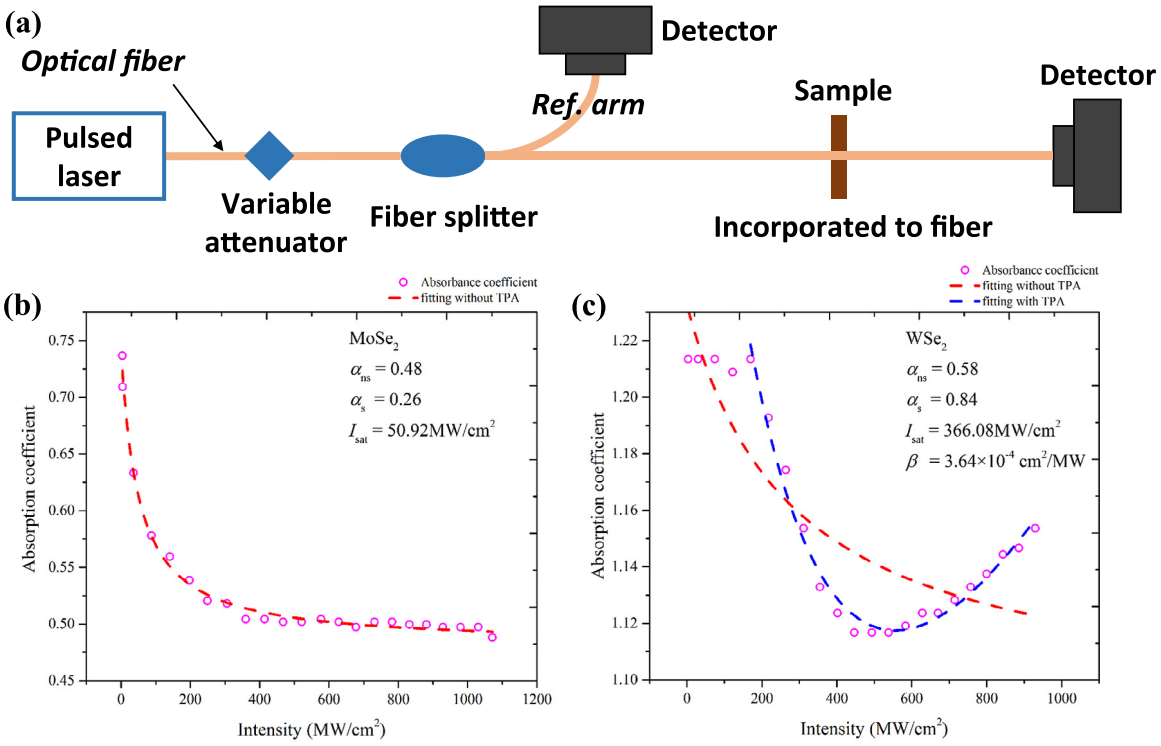

Fig. 5. (a) Two-arm measurement setup, (b) a typical two-arm measurement result, and (c) a two-arm measurement result with TPA [26] (with permission of OSA).

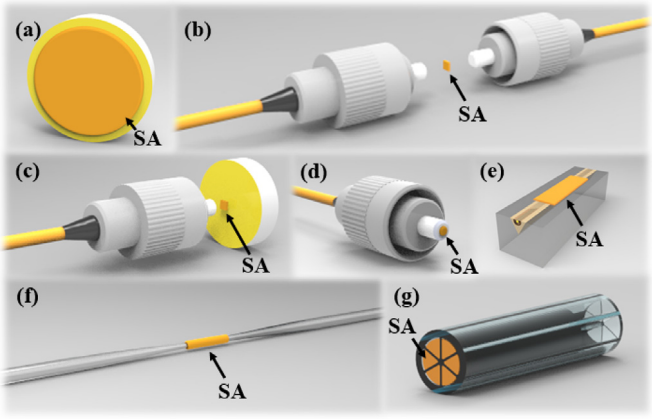

Fig. 6. Incorporation schemes for 2D material saturable absorbers: (a) Transferring SA on substrate for free-space coupling; Sandwiching thin-film SA between (b) two fiber connectors and (c) a fiber connector and a mirror; Transferring or depositing SA on (d) fiber end, (e) side-polished fiber and (f) tapered fiber; (g) Filling SA into a photonic crystal fiber.

all the light beam is confined in the fiber, no spatial information can be collected like closed-aperture Z-scan. Therefore two-arm measurement can only measure saturable absorption of the materials. However, two-arm measurement does not require free space components and fine tuning of the beam path, and thus has much simpler setup than Z-scan measurement. Fig. 5(b) shows a typical measured saturable absorption curve in a two-arm measurement and the saturation process can be seen. Fig. 5(c) shows a typical saturable absorption curve with TPA. Increase of the absorption at high intensity can be observed.

3. Mode-locked and Q-switched lasers based on 2D materials

The abundant photonic and optoelectronic properties of 2D materials have been utilized to realize many photonic devices including modulator, photodetector, polarizer and switch, etc. Meanwhile, pulsed laser technology is an important platform covering a wide dimension from fundamental science to practical industrial application. The saturable absorption of 2D materials provides a pulse shaping mechanism and thus can support pulsed operation in a laser cavity. Various works of pulsed lasers based on 2D material SAs have been reported. In this section, two typical types of pulsed lasers, mode-locked lasers and Q-switched lasers, are discussed.

3.1. SA incorporation

To satisfy the requirement of usage in a laser cavity, fabricated raw 2D materials should be further processed to be incorporated. There are many incorporation designs to "fit" the 2D materials into the laser cavity. Generally, these incorporation designs are different for solid-state lasers and fiber lasers. For solid-state lasers, the coupling between the 2D materials and light beam is usually achieved in free space, which results in a quite simple and straightforward coupling. For fiber lasers,

Table 2
Comparison of different incorporation schemes.

Incorporation schemes	Pure material	Power handling	Scalability	Interaction length
Transferring on substrate for free space coupling	Yes	High	No	Short
Embedding in polymer thin film	No	Low	Yes	Short
Transferring / depositing on fiber end	Yes	Medium	No	Short
Transferring / depositing on side-polished fiber or tapered fiber	Yes	High	No	Long
Filling in PCF	Yes	High	No	Long

Table 3
Performance summary of mode-locked lasers based on TIs, TMDs and BP saturable absorbers.

2D materials		Center wavelength	3-dB bandwidth	Rep. rate	Pulse energy	Output power	Incorporation method	Ref.
TIs	Sb_2Te_3	1039 nm	4.25 nm	17.07 MHz	32 pJ	0.54 mW	Deposited on side-polished fiber	[34]
		1542 nm	63 nm	95.4 MHz	660.4 pJ	63 mW	Deposited on tapered fiber	[61]
		1558 nm	17 nm	1.75 MHz	–	–	Deposited on side-polished fiber	[34]
		1558 nm	34 nm	25.38 MHz	0.1–0.21 nJ	2.6–5.34 mW	Deposited on side-polished fiber	[33]
		1561 nm	8.5 nm	26.53 MHz	37.7 pJ	1 mW	Deposited on side-polished fiber	[34]
		1565 nm	37 nm	22.4 MHz	44.6 pJ	1 mW	Deposited on side-polished fiber	[34]
		1565 nm	30 nm	22.32 MHz	44.8 pJ	1 mW	Deposited on side-polished fiber	[15]
	Bi_2Se_3	1065 nm	1.11 nm	1.11 MHz	1.08 nJ	1.2 mW	PCF filled with TI nanosheets	[62]
		1530 nm	–	8.95 MHz	–	–	Deposited on fiber end	[63]
		1554.6 nm	7.91 nm	202.7 MHz	3.95 pJ	0.8 mW	PCF filled with TI nanosheets	[64]
		1557–1600 nm	7.76 nm	46.4 MHz	–	–	Deposited on fiber end	[65]
		1557–1565 nm	1.79 nm	1.21 MHz	–	–	Polymer thin film	[3]
		1557 nm / 1559 nm	1.12 nm/ 1.75 nm	388 MHz (HML) / 239 MHz (HML)	–	–	Deposited on tapered fiber	[19]
		1558 nm	4.3 nm	12.5 MHz	0.144 nJ	1.8 mW	Polymer thin film	[20]
		1559 nm	26 nm	7.04 MHz	10.65 nJ	75 mW	PCF filled with TI nanosheets solution	[64]
		1562 nm	0.5 nm	9.75 MHz	–	–	Polymer thin film	[66]
		1600 nm	7.9 nm	35.45 MHz	24.26 pJ	0.86 mW	Polymer thin film	[67]
		1610 nm	1.06 nm	7.04 MHz	43.8 nJ	308 mW	Deposited on tapered fiber	[68]
	Bi_2Te_3	1058 nm	3.69 nm	1.44 MHz	0.599 nJ	0.86 mW	Deposited on side-polished fiber	[69]
		1545 nm	32.5 nm	31 MHz	0.06 nJ	2 mW	Deposited on side-polished fiber	[70]
		1547 nm	4.63 nm	15.11 MHz	52.9 pJ	0.8 mW	Deposited on side-polished fiber	[13]
		1548–1571 nm	35.95–51.62 nm	10.71 MHz	1.03 nJ	11 mW	Polymer thin film	[58]
		1556 nm	4.5 nm	14.07 MHz / 773.85 MHz (HML)	1.32–2.52 pJ	1.3 mW	Deposited on side-polished fiber	[71]
		1556 nm	6 nm	22.13 MHz	39.6 pJ	0.9 mW	Deposited on side-polished fiber	[4]
		1559 nm	1.88 nm	3.75 MHz / 304 MHz (HML)	133 pJ	65 mW	Deposited on fiber end	[14]
		1559 nm	0.95 nm/1.08 nm	4.88 MHz / 2.04 GHz (HML)	2.46–65.6 pJ	0.32–5.02 mW	Deposited on tapered fiber	[18]
		1561 nm	9.15 nm	18.55 MHz	27 pJ	0.5 mW	Deposited on tapered fiber	[32]
		1562 nm	8.2 nm/5.6 nm	17.34 MHz / 2.95 GHz (HML)	32 pJ/26.7 pJ	0.56 mW / 45.3 mW	Deposited on tapered fiber	[72]
		1916 nm	3.6 nm	21.5 MHz / 215 MHz (HML)	28.8–93 pJ	2–6.2 mW	Deposited on tapered fiber	[73]
		1935 nm	5.64 nm	27.9 MHz	0.717 nJ	20 mW	Deposited on side-polished fiber	[74]
TMDs	MoS_2	1038 nm	0.9 nm	15.43 MHz	97 pJ	1.5 mW	Polymer thin film	[75]
		1063 nm	0.1 nm	2.17 MHz	4.53 nJ	9.84 mW	Polymer thin film	[76]
		1064 nm	0.34 nm	88.3 MHz	1.0 nJ	89 mW	Deposited on mirror	[77]
		1056–1074 nm	~0.5 nm	2.67 MHz	–	2.6 mW	Deposited on mirror	[23]
		1530 nm	2.1 nm	8.968 MHz / 125 MHz (HML)	–	–	Deposited on side-polished fiber	[78]
		1535–1565 nm	–	–	65 pJ	–	Polymer thin film	[79]
		1557 nm / 1558 nm	2.47 nm / 0.94 nm	6.77 MHz / 2.5 GHz (HML)	–	65 μW / 2.51–5.39 mW	Deposited on tapered fiber	[80]
		1556 nm	6.1 nm	463 MHz	–	5.9 mW	Polymer thin film	[57]
		1557 nm	–	5.05 MHz	–	–	Deposited on tapered fiber	[81]
		1590 nm	11.7 nm	7.45 MHz	–	6.91 mW	Deposited on side-polished fiber	[82]
		1568 nm	2.3 nm	5.78 MHz	–	–	Polymer thin film	[21]
		1568 nm	12.38 nm	33.48 MHz	–	–	Deposited on side-polished fiber	[83]
		1568 nm	23.2 nm	26.02Mhz	–	–	Deposited on side-polished fiber	[83]
		1569 nm	2.6 nm	8.288 MHz	0.615 nJ	5.1 mW	Polymer thin film	[31]
		1570 nm	2.7 nm	5.924 MHz	0.59 nJ	3.5 mW	Polymer thin film	[84]
		1905 nm	17.3 nm	9.67 MHz	15.5 nJ	150 mW	Deposited on mirror	[25]
	WS_2	1030 nm	1.1 nm	2.84 MHz	2.82 nJ	8.02 mW	Polymer thin film	[24]
		1052 nm	0.29 nm	23.26 MHz	–	30 mW	Polymer thin film	[85]
		1058 nm	2.1 nm	86.7 MHz	–	270 mW	Deposited on mirror	[49]
		1064 nm	0.77 nm	5.57 MHz	1.36 nJ	7.6 mW	Deposited on side-polished fiber	[8]
		1530 nm	4.8 nm	116.5 MHz	–	–	Deposited on tapered fiber	[86]
		1550 nm	0.0314 nm	396 MHz	–	4.46 mW	Deposited on mirror	[87]

(*continued on next page*)

Table 3 (*continued*)

2D materials		Center wavelength	3-dB bandwidth	Rep. rate	Pulse energy	Output power	Incorporation method	Ref.
		1557 nm / 1564 nm	4 nm / 3.9 nm	10.2 MHz / 460.7 MHz (HML)	–	–	Deposited on side-polished fiber	[88]
		1557 nm	2.3 nm	8.86 MHz	12.4 pJ	110 mW	Deposited on side-polished fiber	[89]
		1557 nm	3.1 nm	8.96 MHz	–	–	Polymer thin film	[89]
		1559 nm / 1558 nm	3.2 nm/ 3.4 nm	14.57 MHz / 1.51 GHz (HML)	2.3 pJ / 1.39 pJ	- / 2.08 mW	Deposited on side-polished fiber	[90]
		1560 nm	11.48 nm	8.83 MHz	1.14 nJ	10.1 mW	Deposited on tapered fiber	[35]
		1560 nm	6.75 nm	19.57 MHz	76.6pJ	1.5 mW	Deposited on tapered fiber	[36]
		1560 nm	0.031 nm	352 MHz	–	5.28mw	Deposited on mirror	[36]
		1561 nm	7.5 nm	24.93 MHz	–	1.93 mW	Deposited on tapered fiber	[91]
		1563 nm	5.2 nm	20.39 MHz	–	2.77 mW	Deposited on tapered fiber	[91]
		1563 nm	5.71 nm	9.76 MHz	–	–	Deposited on tapered fiber	[92]
		1565 nm	8.23 nm	31.11 MHz	–	–	Deposited on side-polished fiber	[93]
		1566 nm	14.5 nm	8.05 MHz	0.22 nJ	1.7 mW	Deposited on side-polished fiber	[8]
		1572 nm	5.2 nm	–	–	–	Polymer thin film	[28]
		1941 nm.	5.6 nm	34.8 MHz	17.2 pJ	0.6 mW	Deposited on side-polished fiber	[94]
	WSe_2	1557 nm / -	2 nm / -	5.31 MHz / 3.25 GHz (HML)	–	- / 19 mW	Deposited on side-polished fiber	[95]
		1558 nm	2.1 nm	5.31 MHz	–	–	Polymer thin film	[95]
	$MoSe_2$	1556 nm / 1557 nm	5.4 nm / 5.1 nm	15.38 MHz / 3.27 GHz (HML)	14.6 pJ / 5.9 pJ	0.23 mW / 22.8 mW	Deposited on side-polished fiber	[96]
		1557 nm	2.3 nm	5.03 MHz	–	–	Deposited on side-polished fiber	[95]
		1558 nm	1.76 nm	8.028 MHz	54.8 pJ	440 μW	Polymer thin film	[97]
		1560 nm	7.8 nm	8.8 MHz	91.3 pJ	–	Polymer thin film	[17]
		1563 nm	2.2 nm	5.03 MHz	–	–	Polymer thin film	[95]
	$MoTe_2$	1555 nm	2 nm	–	–	–	Polymer thin film	[98]
		1561 nm	2.4 nm	5.26 MHz	–	–	Deposited on side-polished fiber	[98]
	WTe_2	1555 nm	2 nm	–	–	–	Deposited on side-polished fiber	[98]
		1556 nm	4.14 nm	13.98 MHz	–	0.04 mW	Polymer thin film / deposited on side-polished fiber	[99]
		1565 nm	2 nm	–	–	–	Polymer thin film	[98]
BP	–	1053 nm	4.65 nm	63.3 MHz	6.48 nJ	0.82 W	Deposited on mirror	[100]
		1064 nm	0.288 nm	140 MHz	3.29 nJ	460 mW	Deposited on mirror	[101]
		1086 nm	0.23 nm	13.5 MHz	5.93 nJ	80 mW	Deposited on fiber end	[102]
		1555 nm	4.6 nm	37.8 MHz	–	–	Deposited on fiber end	[103]
		1558 nm	1.25 nm	15.59 MHz	–	77.6 μW	Deposited on side-polished fiber	[104]
		1559 nm	6.2 nm	14.7 MHz	–	1.6 mW	Deposited on fiber end	[105]
		1559 nm	6.2 nm.	14.7 MHz	–	–	Deposited on fiber end	[106]
		1560 nm	3.8 nm	8.77 MHz	–	–	Deposited on fiber end	[107]
		1560 nm	10.2 nm	28.2 MHz	–	0.5 mW	Deposited on fiber end	[108]
		1561 nm	6.4 nm	6.88 MHz	0.74 nJ	5.1 mW	Deposited on fiber end	[109]
		1532–1570 nm	3.39 nm	4.96 MHz	–	5.6 mW	Deposited on tapered fiber	[110]
		1568 nm	0.52 nm	1.843 MHz	–	4.43 mW	Deposited on fiber end	[111]
		1549–1575 nm	9.35 nm	60.5 MHz	–	–	Deposited on tapered fiber	[112]
		1571 nm	2.9 nm	5.96 MHz	–	–	Deposited on fiber end	[11]
		1898 nm	3.9 nm	19.2 MHz	–	0.07 – 8.45 mW	Deposited on tapered fiber	[113]
		1910 nm	5.8 nm	36.8 MHz	–	1.5 mW	Deposited on fiber end	[108]
		1910 nm	5.8 nm	36.8 MHz	40.7 pJ	1.5 mW	Deposited on fiber end	[114]
		2783 nm	2.8 nm	24.27 MHz	25.5nJ	613 mW	Deposited on mirror	[115]
		2867 nm	4.35 nm	13.987 MHz	6.28 nJ	87.8 mW	Deposited on mirror	[116]

HML: harmonic mode locking

the coupling should consider the unique fiber property and many special designs have been developed. Fig. 5 summarizes a few popular designs.

In Fig. 6(a), the 2D material is transferred to a plain substrate for free-space coupling in solid-state lasers. For CVD grown 2D materials, the transfer process is consisted of a few steps including coating polymer on the materials, removing the original substrate by chemical etching, transferring the 2D material-polymer thin film onto the target substrate, and removing the polymer by acetone. The new substrate can be transparent in the laser operation wavelength for transmission coupling or a mirror for reflective coupling [25,54,55].

For the material incorporation in fiber lasers, a simple method is to embed 2D materials to polymer thin film. The polymer can be PVA [16,24,26–28,56,57], PMMA [58] or others. The thickness of the thin film is around a few tens of micrometer [26–28,56–59]. Because the fiber cores are usually very small, e.g., ~9 μm for standard single mode fiber near 1550 nm, one round of fabrication of a 1×1 cm thin film can be cut into tens of individual saturable absorber thin films. The small SA thin film can be sandwiched between two fiber connectors for transmission coupling, shown in Fig. 6(b) or between a fiber connector and a mirror for reflective coupling, shown in Fig. 6(c). Although polymer thin film is a very convenient substrate for 2D materials, its low thermal stability is a main concern for practical applications. High average power [26] or high instant peak power [56] in the fiber can all change the property of the polymer and even damage the saturable absorbers. This propels researchers to find other methods to incorporate pure 2D materials into laser cavities. Direct transfer from CVD grown

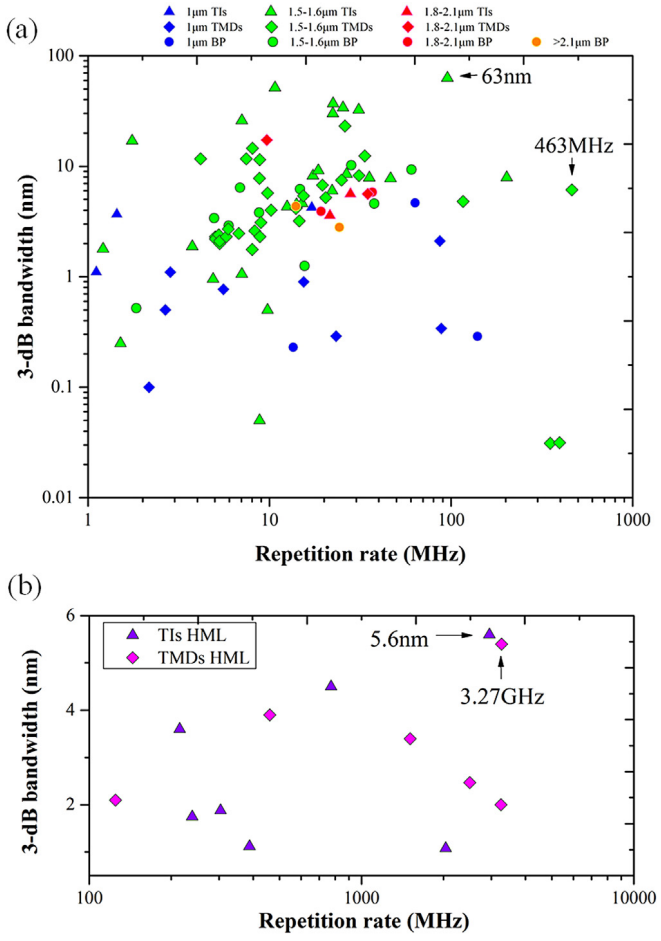

Fig. 7. 3-dB bandwidth versus repetition rate of 2D materials based mode-locked lasers, (a) fundamental mode locking, and (b) harmonic mode locking.

2D materials is an approach. The detailed process is nearly identical to the process described above for free-space coupling in Fig. 6(a). This method can transfer 2D materials to fiber end, side-polished fiber and tapered fiber, shown in Fig. 6(d)-(f). Another approach is optical driven deposition. By putting fiber into the dispersions of 2D materials (e.g., prepared by LPE method) and injecting light, leaked light field from the fiber can attract 2D material nanosheets in the dispersions and attach them to the fiber. This method can also deposit 2D materials to fiber end, side-polished fiber and tapered fiber. By monitoring the instant power in the fiber, the deposition process can be controlled to deposit proper amount of 2D materials to the fiber. By using solvent with volatility, e.g., ethanol, laser power down to a few dBm has been reported to drive the deposition [60]. For the 2D materials transferred/deposited on side-polished fiber and tapered fiber, only the evanescent field of the light beam in the fiber interacts with the materials which reduces the light intensity in the materials and prevents the materials from thermal damage. Also, side-polished fiber and tapered fiber allow a very long interaction length and therefore are preferred platforms in many experiments investigating optical nonlinearity. The last method is to use photonic crystal fiber (PCF). By filling 2D materials into the hollow channels in a PCF, a saturable absorber can be formed, shown in Fig. 6(g). This method also allows a long interaction length between 2D materials and light beam, but the coupling between PCF and standard fiber is still challenging.

A comparison of the above incorporation schemes is listed in Table 2. It should be noted that there is no incorporation scheme which is absolutely better than others. Instead, proper incorporation schemes should be chosen based on applications.

3.2. Mode-locked lasers

Mode-locked lasers generate ultrashort pulses in time domain with wide spectrum in frequency domain. To obtain mode locking operation, a pulse shaping mechanism is needed in the laser cavity, i.e., pulsed operation should experience higher net gain than continuous wave (CW) operation so that CW operation can be suppressed and pulsed operation prevails in the gain competition. Pulse shaping mechanism can be active by using an optical modulator in the laser cavity and manually applying a periodic high transmission window in time domain, or passive by using a passive device, known as saturable absorber, in the cavity to let the laser operates in the pulsed mode by itself. A SA exhibits low absorption at high input optical intensity and high absorption at low intensity. When a pulse propagates through a SA, the pulse peak experiences lower loss while the pulse wing experiences higher loss. Therefore the pulse is narrowed by the SA every time it propagates through the SA until the pulse narrowing (Kerr nonlinearity in the cavity may also contribute)

Table 4
Bandgaps and demonstrated longest operation wavelength of TIs, TMDs and BP.

2D materials		Bandgaps	Longest operation wavelength in lasers
TIs	Sb_2Te_3	Gapless for surface state band Indirect for bulk: ~0.07 eV (17.7 μm) [117]	1565 nm [15]
	Bi_2Se_3	Gapless for surface state band Indirect for bulk: ~0.3 eV (4.14 μm) [117]	1610 nm [68]
	Bi_2Te_3	Gapless for surface state band Indirect for bulk: ~0.06 eV (20.7 μm) [117], ~0.165 eV (7.53 μm) if doped [118]	1935 nm [74]
TMDs	MoS_2	Direct for monolayer: ~1.8 eV (690 nm) [119] Indirect for bulk: ~1.29 eV (963 nm) [119]	1905 nm [25]
	WS_2	Direct for monolayer: ~2.1 eV (592 nm) [120] Indirect for bulk: ~1.3 eV (956 nm) [120]	1941 nm [94]
	WSe_2	Direct for monolayer: ~1.65 eV (753 nm) [43] Indirect for bulk: ~1.2 eV (1035 nm) [43]	1558 nm [95]
	$MoSe_2$	Direct for monolayer: ~1.57 eV (791 nm) [43] Indirect for bulk: ~1.1 eV (1129 nm) [43]	1560 nm [17]
BP	–	Direct for mono- and few-layer: 0.3–1.5 eV (4140–827 nm) depending on number of layers [121]	2867 nm [116]

Table 5
Extreme specifications on repetition rate, 3-dB bandwidth, pulse energy and boundary of operation wavelength in mode-locked lasers based on TIs, TMDs and BP SAs.

Specifications	Values	Other specifications of the lasers	Ref.
Repetition rate	463 MHz (Fundamental ML)	Center wavelength 1556 nm, 3-dB bandwidth 6.1 nm, output power 5.9 mW, SA MoS_2 in polymer thin film	[57]
	3.27 GHz (Harmonic ML)	Center wavelength 1556 nm, 3-dB bandwidth 5.1 nm, output power 22.8 mW, SA $MoSe_2$ deposited on side-polished fiber	[96]
3-dB bandwidth	63 nm	Center wavelength 1542 nm, repetition rate 95.4 MHz, output power 63 mW, SA Sb_2Te_3 deposited on tapered fiber	[61]
Pulse energy	25.5 nJ	Center wavelength 2783 nm, 3-dB bandwidth 2.8 nm, repetition rate 24.27 MHz, output power 613 mW, SA BP deposited on mirror	[115]
Shortest wavelength	1030 nm	3-dB bandwidth 1.1 nm, repetition rate 2.84 MHz, output power 8.02 mW, SA WS_2 in polymer thin film	[24]
Longest wavelength	2867 nm	3-dB bandwidth 4.35 nm, repetition rate 13.987 MHz, output power 87.8 mW, SA BP deposited on mirror	[116]

ML: mode locking

is balanced by the pulse broadening in the cavity (e.g., induced by dispersion) and a stable pulsed operation is obtained.

There are usually two methods to obtain saturable absorbers. One is based on Kerr nonlinearity including Kerr lens, nonlinear polarization evolution (NPE), nonlinear optical loop mirror (NOLM), nonlinear amplified loop mirror (NALM), etc. These methods are also known as artificial saturable absorbers. The other is based on material property. As described in Section 2.3, when there are many incident photons shining on a certain material, many electrons are excited to the conduction band until the conduction band is completely filled and no more photons can be absorbed. As long as a material has a proper bandgap to allow the absorption of photons with certain wavelength, it can be considered as a saturable absorber. Many semiconductor materials have been demonstrated saturable absorption including III-V materials, nanoparticles and of course 2D materials. Here we focus our discussion on three typical newly emerged 2D materials –topological insulators, transition metal dichalcogenides and black phosphorus (also known as phosphorene).

Table 3 summarizes the reported optical performance of the mode-locked lasers based on TIs, TMDs and BP saturable absorbers. These data are also plotted in Fig. 7 with the horizontal axis representing repetition rate and the vertical axis representing 3-dB bandwidth. In the figure, marker shapes represent different materials and marker colors represent different operation wavelengths of the lasers.

An interesting observation is that the operation wavelength of these mode-locked lasers based on TIs, TMDs or BP SAs covers a wide spectral region from ~1 μm to ~2.9 μm. Table 4 lists the bandgaps of these materials and the longest wavelengths demonstrated in mode-locked lasers. For TIs and BP, there is no problem because their bandgaps are small enough. But for TMDs, the demonstrated operation wavelengths in lasers are even longer than the cut-off wavelengths defined by their bandgaps. This phenomenon is usually attributed to the absorption induced by the edge states or localized excitation of 2D materials. The existence of edge states creates sub-bandgaps with much smaller excitation photon energy and thus allows the absorption of photons with energy lower than the normal bandgaps. A thorough investigation is still required to better understand this phenomenon.

We go back to our focus on the performance of the mode-locked lasers based on these three types of 2D materials. A few parameters are paid attention. They are repetition rate, 3-dB bandwidth, pulse energy, and boundary of operation wavelength. Repetition rate is a key parameter for high-speed applications such as optical sampling. A mode-locked laser with high repetition rate is always desired to extend the system speed. 3-dB bandwidth determines how much spectrum can be utilized in the spectrum related applications such as arbitrary waveform generation. It also determines the transform-limited pulse width. Pulse energy is important in the investigation of optical nonlinearity and determines the maximum peak power for a given pulse duration. The boundary of operation wavelength indicates the capability of broadband operation of 2D materials. These parameters are summarized in Table 5.

In short, mode-locked lasers based on TIs, TMDs and BP SAs have been able to operate in a wide range of wavelength, obtain broad optical spectrum, and generate high-repetition-rate pulse train and high-energy pulses, which is partially comparable to the current specifications of the mode-locked lasers based on other technologies. By further optimizing the SA design and laser cavity parameters, mode-locked lasers based on TIs, TMDs, and BP SAs are expected to achieve even higher performance.

3.3. Q-switched lasers

Q-switched lasers are another kind of pulsed lasers. Different from mode-locked lasers which generate ultrashort pulses (ps-fs) and wide optical spectrum, Q-switched lasers generates wider pulses (μs-ns) and higher pulse energy. The technology of obtaining Q-switching operation is however quite similar to that used for mode-locked lasers. Q-switching operation can be achieved actively by inserting an optical modulator in the cavity, or passively by inserting saturable absorbers in the cavity. For passive case, whether a cavity with SA supports Q-switching operation or mode locking operation is both dependent on the property of cavity and the property of SA. Ref.[122] has provided a very detailed discussion on the different operation modes in a laser.

Table 6 summarizes the reported optical properties from the Q-switched lasers based on TIs, TMDs and BP saturable absorbers. Similarly, we also plot these data in Fig. 8 with the horizontal axis representing repetition rate and the vertical axis representing pulse energy. In the figure, marker shapes represent different materials and marker colors represent different operation wavelengths of the lasers.

Similarly, we focus on some important parameters of the Q-switched lasers. They are repetition rate, pulse energy, pulse width and boundary of operation wavelength. Table 7 summarizes the best performance of these parameters.

In short, Q-switched lasers based on TIs, TMDs or BP SAs have been able to operate in a wide range of wavelength, obtain high pulse energy and narrow pulse width, and generate high-repetition-rate pulse train. Higher performance is expected if further optimization is applied to the SA and laser cavity design.

4. Conclusions and future perspective

In this paper, the properties of 2D materials and pulsed lasers based on three 2D materials TIs, TMDs and BP have been reviewed. For material properties, fabrication, characterization and optical nonlinearity are discussed. For pulsed lasers, we focus on mode-locked lasers and Q-switched lasers based on 2D material saturable absorbers. A detailed summary of currently reported works is provided and the best performance on some specifications of these lasers is highlighted. For example, for mode-locked lasers, the repetition rate has reached 463 MHz for fundamental mode locking and 3.27 GHz for harmonic mode locking, the optical spectrum has reached 63 nm and the pulse energy has reached 25.5 nJ. For Q-switched lasers, the repetition rate has reached more than 3 MHz, the pulse energy has reached 39.5μJ and the pulse width has been down to 433 ps. Moreover, the operation wavelength has covered an ultra-wide range from visible (604 nm) to mid-IR (2970 nm). Therefore, it can be concluded that mode-locked and Q-switched lasers based on TIs, TMDs and BP have been partially comparable to the lasers using other saturable absorbers which have been developed for more than twenty years while SAs based on 2D materials have just been investigated for less than ten years.

Table 6
Performance summary of Q-switched lasers based on TIs, TMDs and BP saturable absorbers.

2D materials		Center wavelength	Pulse energy	Rep. rate	Pulse width	Output power	Incorporation method	Ref.
TI	Bi_2Se_3	635.5 nm	22.3 nJ	191.6 –454.5 kHz	244 ns	7.6 mW	Deposited on fiber end	[123]
		1067 nm	17.9 nJ	8.3–29.1 kHz	1.95 μs	0.46 mW	Deposited on fiber end	[7]
		1313 nm	1.23 μJ	161.3 kHz	433 ns	200 mW	Polymer thin film (BK7 glass)	[124]
		1511–1589 nm	1.5 μJ	2.15–12.8 kHz	13 μs	19.56 mW	Deposited on fiber end	[5]
		1543 nm	3.4–4 nJ	2.6–12 kHz	9.5–50 μs	15–42 μW	Deposited on tapered fiber	[125]
		1545–1565 nm	11.4–13.3 nJ	4.5–12.9 kHz	13.4–36 μs	99–112 μW	Deposited on fiber end	[126]
		1565 nm	23.8 nJ	495–940 kHz	1.9–7.79 μs	22.35 mW	Polymer thin film	[6]
		1645 nm	5.3 μJ	40.7 kHz	6.3 μs	210 mW	Polymer thin film	[127]
		1890 nm	11.54 nJ	35–60 kHz	1.71–3.54 μs	0.68 mW	Deposited on side-polished fiber	[128]
		1980 nm	313 nJ	8.4–26.8 kHz	4.18 μs	84 mW	Deposited on fiber end	[129]
		2800 nm	9.3 μJ	92 kHz	1.3 μs	856 mW	Polymer thin film	[59]
	Bi_2Te_3	1056 nm	38.3 nJ	35–77 kHz	1–1.3 μs	2.95 mW	Deposited on side-polished	[130]
TMDs	MoS_2	604 nm	5.5nJ	50.8–118.4 kHz	602 ns	0.6 mW	Polymer thin film	[131]
		636 nm	–	240.4–438.6 kHz	227 ns	7.1 mW	Polymer thin film	[132]
		978 nm	–	221 kHz	0.63 μs	127 mW	Deposited on mirror	[133]
		1030–1070 nm	100 nJ	74 kHz	2.88 μs	–	Polymer thin film	[119]
		1060 nm	32.6 nJ	6.4–28.9 kHz	5.8 μs	–	Polymer thin film	[134]
		1064 nm	174.7 nJ	1.25 MHz	164 ns	218.4 mW	Deposited on mirror	[135]
		1068 nm	–	–	2.7 μs	–	Polymer thin film	[136]
		1550 nm	152 nJ	131 kHz	660 ns	–	Deposited on mirror	[137]
		1520–1568 nm	160 nJ	8.77–43.47 kHz	26.7 to 3.3 μs	5.91 mW	Polymer thin film	[22]
		1560 nm	184.7 nJ	41.452 kHz	9.92 μs	0.77 mW	Polymer thin film	[26]
		1560 nm	63.2 nJ	6.5–27.0 kHz	5.4 μs	–	Polymer thin film	[134]
		1567 nm	74.93 nJ	76.56 kHz	4.17 μs	6.47 mW	Polymer thin film	[21]
		1902 nm	2.08 μJ	25.58–48.09 kHz	0.8 μs	100 mW	Polymer thin film (mica)	[138]
		2030 nm	1 μJ	33.6–48.1 kHz	1.76 μs	–	Polymer thin film	[139]
	WS_2	604 nm	6.4 nJ	67.3–132.2 kHz	435 ns	0.7 mW	Polymer thin film	[131]
		635 nm	28.7 nJ	232.7–512.8 kHz	207 ns	8.7 mW	Polymer thin film	[132]
		1030 nm / 1035 nm	–	–	4.6 μs / 4.1 μs	210 μW / 199 μW	Polymer thin film	[140]
		1030 nm	13.6 nJ	36.7 kHz	3.2 μs	0.5 mW	Polymer thin film	[141]
		1030–1070 nm	126 nJ	–	2.88 μs	–	Polymer thin film	[79]
		1048 nm	–	97.0 kHz	1.58 μs	–	Polymer thin film	[142]
		1064 nm	–	45.25 kHz	1.28 μs	52 mW	Polymer thin film	[143]
		1558 nm	19 nJ	82–134 kHz	0.71 μs	2.5 mW	Deposited on side-polished fiber	[120]
		1558 nm	179.6 nJ	97 kHz	1.1 μs	16.4 mW	Polymer thin film	[141]
		1560 nm	1179.4 nJ	77.925 kHz	6.707 μs	6.41 mW	Polymer thin film	[26]
		1560 nm	54.4 nJ	296.7 kHz	160 ns	17.3 mW	Deposited on mirror	[36]
		1560 nm	68.5 nJ	367.8 kHz	154.9 ns	25.2 mW	Deposited on mirror	[144]
		1561 nm	11nJ	84.8 kHz	1.44 μs	0.3 mW	Deposited on fiber end	[145]
		1562 nm	–	77 kHz	4.1 μs	–	Polymer thin film	[146]
		1565 nm	–	108 kHz	3 μs	7.84 mW	Deposited on tapered fiber	[147]
		1570 nm	46.3 nJ	90–125 kHz	–	–	Polymer thin film	[28]
		2866 nm	0.37 μJ	131.6 kHz	1.73 μs	48.4 mW	Deposited on mirror	[54]
	WSe_2	1064 nm	19 nJ	2.938 MHz	52 ns	45.7 mW	Deposited on mirror	[148]
		1560 nm	17 nJ	26.907 kHz	3.976 μs	0.46 mW	Polymer thin film	[149]
		1560 nm	23 nJ	112.23 kHz	1.013 μs	2.66 mW	Polymer thin film	[50]
		1560 nm	484.8 nJ	85.365 kHz	9.182 μs	3.16 mW	Polymer thin film	[26]
	$MoSe_2$	635 nm	–	357.1–555.1 kHz	240 ns	6.2 mW	Polymer thin film	[132]
		1060 nm	825 nJ	29.4 kHz	5.65 μs	24.5 mW	Polymer thin film	[150]
		1064 nm	35.9 nJ	3.334 MHz	86 ns	115.1 mW	Deposited on mirror	[148]
		1560 nm	369.5 nJ	66.847 kHz	6.506 μs	2.45 mW	Polymer thin film	[26]
		1562 nm	57.9 nJ	32.8 kHz	30.4 μs	1.9 mW	Polymer thin film	[151]
		1566 nm	116 nJ	65.0 kHz	2.85 μs	8.0 mW	Polymer thin film	[150]
		1924 nm	42 nJ.	16.9 kHz	7.11 μs	0.79 mW	Polymer thin film	[150]
BP	–	635 nm	27.6 nJ	409.8 kHz	383 ns	4.4 mW	Deposited on mirror	[152]
		639 nm	104 nJ	172 kHz	189 ns	18 mW	Deposited on mirror	[11]
		1029 nm	0.09 μJ	63.9 kHz	1.73 μs	6 mW	Deposited on mirror	[153]
		1039 nm / 1042 nm	2.09 nJ	52.52–58.73 kHz	1.16 μs	0.12 mW	Deposited on fiber end	[154]
		1046 nm	325.7 nJ	113.6 kHz	620 ns	37 mW	Deposited on mirror	[155]
		1057–1083 nm	7.1 nJ	6.0–44.8 kHz	4 μs	0.3 mW	Deposited on fiber end	[156]
		1060 nm	70.4 nJ	312 kHz	495 ns	22 mW	Deposited on mirror	[157]
		1069 nm	328 nJ	32.9 kHz	10.8 μs	10 mW	Deposited on fiber end	[158]
		1533 nm	18.6 nJ.	40 kHz	3.1 μs	728 μW	Deposited on fiber end	[105]
		1533 nm	18.2 nJ	40 kHz	3.16 μs	728 μW	Deposited on fiber end	[106]
		1550 nm	28.3 nJ	4.43–18 kHz	31–9.35 μs	500 μW	Deposited on side-polished fiber	[159]
		1557 nm	142.6 nJ	5.73–31.07 kHz	25.77–63.59 μs	4 mW	Polymer thin film	[160]
		1562 nm	194 nJ	7.86–34.32 kHz	2.96 μs	6.67 mW	Polymer thin film	[161]
		1563 nm	94.3 nJ	15.78 kHz	10.32 μs	1.5 mW	Deposited on fiber end	[11]

(*continued on next page*)

Table 6 (*continued*)

2D materials	Center wavelength	Pulse energy	Rep. rate	Pulse width	Output power	Incorporation method	Ref.
	1832 nm	75 nJ	20–25.5 kHz	4–6.67 μs	–	Deposited on side-polished fiber	[159]
	1860 nm	80.8 nJ	26.4–73 kHz	3.1–4.2 μs	–	Deposited on side-polished fiber	[159]
	1890 nm	276 nJ	24–57.2 kHz	2.53–4.8 μs	–	Deposited on side-polished fiber	[159]
	1912 nm	632.4 nJ	113.3 kHz	731 ns	71.7 mW	Deposited on fiber end	[162]
	1920 nm	238 nJ	14–60 kHz	3–4.7 μs	–	Deposited on side-polished fiber	[159]
	1930 nm	0.68 μJ	17.7 kHz	3.1 μs	12 mW	Deposited on mirror	[153]
	1935 nm	114 nJ	20–42 kHz	4.9–5.7 μs	–	Deposited on side-polished fiber	[159]
	1979 nm	39.5 μJ	81 kHz	181 ns	3.1 W	Deposited on mirror	[163]
	1988 nm	7.84 μJ	19.25 kHz	1.78 μs	151 mW	Deposited on mirror	[164]
	1991 nm	12.03 μJ	17.21 kHz	2.25 μs	207 mW	Deposited on mirror	[164]
	2009 nm	3.32 μJ	11.6 kHz	3.12 μs	38.5 mW	Deposited on mirror	[165]
	2100 nm	221nJ	122 kHz	636 ns	27 mW	Deposited on mirror	[157]
	2411 nm	205 nJ	176 kHz	189 ns	36 mW	Deposited on mirror	[166]
	2720 nm	0.48 μJ	12.6 kHz	4.47 μs	6 mW	Deposited on mirror	[153]
	2779 nm	7.7 μJ	63 kHz	1.18 μs	485 mW	Deposited on mirror	[167]
	2970 nm	4.93 μJ	62.5 kHz	2.41 μs	308.7 mW	Deposited on mirror	[116]

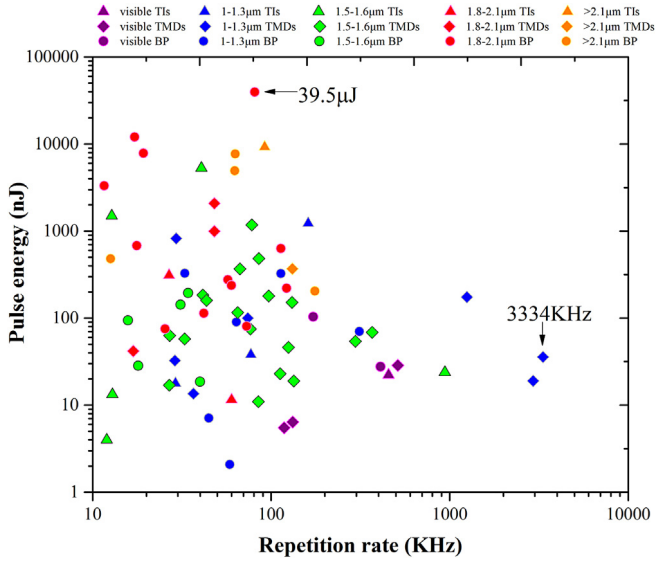

Fig. 8. Pulse energy versus repetition rate of 2D materials based Q-switched lasers.

As future perspective, four aspects may be considered to further improve the laser performance based on 2D materials. They are 1) high speed and low noise, 2) high power and high energy, 3) wide operation spectrum, and 4) spatially inhomogeneous polarization.

4.1. High speed and low noise

Broadband and high-accuracy optical signal processing requires high-speed and low-noise operation of pulsed lasers. For example a photonic analog-to-digital conversion (ADC) system has required a fundamental repetition rate up to GHz and a timing jitter down to a few fs to achieve high-performance ADC better than its electronic competitors. 2D material based SAs have advantages in both two sides. These SAs allow very short interaction length down to only a few tens of micrometer which enables very compact laser cavity design noting that artificial SA based on fiber nonlinearity usually requires tens of centimeter to accumulate enough phase shift. Moreover, 2D materials have ultrafast decay time down to ~100 fs level [9] which, compared with traditional III-V semiconductor SAs with ps-level decay time, allows much weaker noise coupling induced by the slow saturable absorber effect in the cavity [168]. For example, for high-speed mode-locked lasers, a linear cavity can be constructed and a 2D material based SA can be incorporated as one end mirror of the cavity. By using highly doped gain fiber, total cavity length can be only a few centimeters long and repetition rate up to GHz can be obtained. For low-noise operation, the non-saturable loss of 2D materials based SAs should be optimized to a very low level so that cavity net loss won't be increased to much when the SAs are incorporated. Then the abovementioned noise coupling can be naturally suppressed by 2D material based SAs due to their ultrafast decay time.

4.2. High power and high energy

Scientific research on nonlinear phenomenon requires high peak power and high energy of pulsed lasers. For this application, the peak power and/or pulse energy directly determine the intensity of the optical field applied to the target. High power handling is the key requirement for saturable absorbers. 2D materials also have advantages. Pure 2D materials have very good power handling because they are ultra-thin and heat dissipation is better than bulk materials. To achieve this, high-quality 2D materials should be synthesized and material transfer should be careful to reduce the scattering and non-saturable loss which causes unnecessary heat generation in the material and substrate. A non-oxygen environment may also be considered, especially for BP, by using N_2 to protect the material from oxidation. Moreover, power handling can be further enhanced by utilizing evanescent field based light-matter interaction, e.g., transferring or depositing 2D materials onto side-polished fiber or tapered fiber. If polymer thin film is still preferred for the convenience of usage, some polymer such as fluorine mica with high damage threshold has been reported [85].

4.3. Wide operation spectrum

Different applications require different operating wavelength of lasers. For visible display or communications, SAs should have absorption in visible region. For characterization of chemicals, mid-IR

Table 7
Extreme specifications on repetition rate, pulse energy, pulse width and boundary of operation wavelength in Q-switched lasers based on TIs, TMDs and BP SAs.

Specifications	Values	Other specifications of the lasers	Ref.
Repetition rate	3.334 MHz	Center wavelength 1064 nm, pulse energy 35.9 nJ, pulse width 86 ns, SA $MoSe_2$ deposited on mirror	[148]
Pulse energy	39.5 μJ	Center wavelength 1979 nm, repetition rate 81 kHz, pulse width 181 ns, SA BP deposited on mirror	[163]
Pulse width	52 ns	Center wavelength 1064 nm, pulse energy 19 nJ, repetition rate 2.938 MHz, SA WSe_2 deposited on mirrors	[148]
Shortest wavelength	604 nm	Pulse energy 5.5 nJ / 6.4 nJ, repetition rate 118.4 kHz / 132.2 kHz, pulse width 602 ns / 435 ns, SA MoS_2 / WS_2 in polymer thin film	[131]
Longest wavelength	2970 nm	Pulse energy 4.93 μJ, repetition rate 62.5 kHz, pulse width 2.41 μs, SA BP deposited on mirror	[116]

is a widely used wavelength region and SAs should also work in this region. Thanks to the flexible and tunable bandgaps of different 2D materials, absorption bands combined by different 2D materials have covered a wide spectral range from ~600 nm to ~3 μm. Next step can be to further extend to even shorter wavelength of 400 nm to include full visible region and to extend to longer wavelength (e.g. 5 μm) to include more fingerprint absorption peaks of different chemicals. For example, 400 nm wavelength corresponds to a photon energy of 3.1 eV which is larger than the bandgaps of TMDs, TIs and BP and thus can be absorbed by these materials. If a proper gain medium is utilized at this wavelength, pulsed laser operation at 400 nm is fully possible. For 5 μm wavelength, TIs are gapless for surface states and have very small bandgaps even in bulk which can be used as SAs for mid-IR pulsed lasers. Furthermore, modern material engineering technologies can help to modify the bandgaps of current 2D materials by using heterostructures, doping or patterning and new 2D materials may also be discovered.

4.4. Spatially inhomogeneous polarization

Conventional mode-locked or Q-switched lasers have an output beam with a spatially homogeneous polarization. That is, on the cross section of beam, light in different position all has same polarization. In contrast, a spatially inhomogeneous polarized beam has different polarization in different position on the beam cross section. Beam with spatially inhomogeneous polarization has attracted much attention for its unique properties and important usage in optical trapping and material processing. By inserting a waveplate with specially designed pattern in the laser cavity together with a 2D material based SA, a pulsed output with spatially inhomogeneous polarization can be obtained [169]. It is possible that 2D materials can be directly transferred onto the waveplate to form a multi-functional device as SA and waveplate simultaneously. Moreover, the required pattern may even be directly written on 2D materials using laser direct writing or lithography techniques.

Acknowledgement

This work is partially supported by NSFC (No. 61505105, No. 51302285, No. 61522510, No. 61675217), Shanghai Yangfan Program (No. 14YF1401600), the External Cooperation Program of BIC, CAS (No. 181231KYSB20130007), the "Strategic Priority Research Program" of CAS (No. XDB16030700), and the Key Research Program of Frontier Science, CAS (No. QYZDB-SSW-JSC041).

References

[1] F. Bernard, H. Zhang, S.-P. Gorza, P. Emplit, "Towards mode-locked fiber laser using topological insulators," in Nonlinear Photonics (Optical Society of America), p. NTh1A. 5, 2012.
[2] C. Zhao, H. Zhang, X. Qi, Y. Chen, Z. Wang, S. Wen, D. Tang, Ultra-short pulse generation by a topological insulator based saturable absorber, Appl. Phys. Lett. 101 (2012) 211106.
[3] C. Zhao, Y. Zou, Y. Chen, Z. Wang, S. Lu, H. Zhang, S. Wen, D. Tang, Wavelength-tunable picosecond soliton fiber laser with topological insulator: bi2se3 as a mode locker, Opt. Express 20 (2012) 27888–27895.
[4] J. Boguslawski, J. Sotor, G. Sobon, J. Tarka, J. Jagiello, W. Macherzynski, L. Lipinska, K.M. Abramski, Mode-locked Er-doped fiber laser based on liquid phase exfoliated Sb2Te3 topological insulator, Laser Phys. 24 (2014) 105111.
[5] Y. Chen, C. Zhao, S. Chen, J. Du, P. Tang, G. Jiang, H. Zhang, S. Wen, D. Tang, Large energy, wavelength widely tunable, topological insulator Q-switched erbium-doped fiber laser, IEEE J. Sel. Top. Quantum Electron. 20 (2014) 315–322.
[6] Z. Yu, Y. Song, J. Tian, Z. Dou, H. Guoyu, K. Li, H. Li, X. Zhang, High-repetition-rate Q-switched fiber laser with high quality topological insulator Bi 2 Se 3 film, Opt. Express 22 (2014) 11508–11515.
[7] Z. Luo, Y. Huang, J. Weng, H. Cheng, Z. Lin, B. Xu, Z. Cai, H. Xu, 1.06 μm Q-switched ytterbium-doped fiber laser using few-layer topological insulator Bi 2 Se 3 as a saturable absorber, Opt. Express 21 (2013) 29516–29522.
[8] D. Mao, S. Zhang, Y. Wang, X. Gan, W. Zhang, T. Mei, Y. Wang, Y. Wang, H. Zeng, J. Zhao, WS2 saturable absorber for dissipative soliton mode locking at 1.06 and 1.55 m, Opt. Express 23 (2015) 27509–27519.
[9] K. Wang, J. Wang, J. Fan, M. Lotya, A. O'Neill, D. Fox, Y. Feng, X. Zhang, B. Jiang, Q. Zhao, Ultrafast saturable absorption of two-dimensional MoS2 nanosheets, ACS nano 7 (2013) 9260–9267.
[10] S.B. Lu, L.L. Miao, Z.N. Guo, X. Qi, C.J. Zhao, H. Zhang, S.C. Wen, D.Y. Tang, D.Y. Fan, Broadband nonlinear optical response in multi-layer black phosphorus: an emerging infrared and mid-infrared optical material, Opt. Express 23 (2015) 11183–11194.
[11] Y. Chen, G. Jiang, S. Chen, Z. Guo, X. Yu, C. Zhao, H. Zhang, Q. Bao, S. Wen, D. Tang, Mechanically exfoliated black phosphorus as a new saturable absorber for both Q-switching and Mode-locking laser operation, Opt. Express 23 (2015) 12823–12833.
[12] K.S. Novoselov, A.K. Geim, S.V. Morozov, D. Jiang, Y. Zhang, S.V. Dubonos, I.V. Grigorieva, A.A. Firsov, Electric Field Effect in Atomically Thin Carbon Films, Science 306 (2004) 666–669.
[13] J. Lee, J. Koo, Y.M. Jhon, J.H. Lee, A femtosecond pulse erbium fiber laser incorporating a saturable absorber based on bulk-structured Bi 2 Te 3 topological insulator, Opt. Express 22 (2014) 6165–6173.
[14] J. Sotor, G. Sobon, W. Macherzynski, K. Abramski, Harmonically mode-locked Er-doped fiber laser based on a Sb2Te3 topological insulator saturable absorber, Laser Phys. Lett. 11 (2014) 055102.
[15] J. Sotor, G. Sobon, K.M. Abramski, Sub-130 fs mode-locked Er-doped fiber laser based on topological insulator, Opt. Express 22 (2014) 13244–13249.
[16] L. Li, Y. Wang, H. Sun, L. Duan, X. Wang, J. Si, All-normal dispersion passively mode-locked Yb-doped fiber laser with Bi2Te3 absorber, Opt. Eng. 54 (2015) (046101-046101).
[17] H. Ahmad, S.N. Aidit, N.A. Hassan, M.F. Ismail, Z.C. Tiu, Generation of mode-locked erbium-doped fiber laser using MoSe2 as saturable absorber, Opt. Eng. 55 (2016) (076115-076115).
[18] Z.-C. Luo, M. Liu, H. Liu, X.-W. Zheng, A.-P. Luo, C.-J. Zhao, H. Zhang, S.-C. Wen, W.-C. Xu, 2 GHz passively harmonic mode-locked fiber laser by a microfiber-based topological insulator saturable absorber, Opt. Lett. 38 (2013) 5212–5215.
[19] M. Liu, N. Zhao, H. Liu, X.-W. Zheng, A.-P. Luo, Z.-C. Luo, W.-C. Xu, C.-J. Zhao, H. Zhang, S.-C. Wen, Dual-wavelength harmonically mode-locked fiber laser with topological insulator saturable absorber, IEEE Photonics Technol. Lett. 26 (2014) 983–986.
[20] H. Liu, X.-W. Zheng, M. Liu, N. Zhao, A.-P. Luo, Z.-C. Luo, W.-C. Xu, H. Zhang, C.-J. Zhao, S.-C. Wen, Femtosecond pulse generation from a topological insulator mode-locked fiber laser, Opt. Express 22 (2014) 6868–6873.
[21] Z.-C. Luo, F.-Z. Wang, H. Liu, M. Liu, R. Tang, A.-P. Luo, W.-C. Xu, Pulsed erbium-doped fiber laser by a few-layer molybdenum disulfide saturable absorber: from Q-switching to mode-locking, Opt. Eng. 55 (2016) (081308-081308).
[22] Y. Huang, Z. Luo, Y. Li, M. Zhong, B. Xu, K. Che, H. Xu, Z. Cai, J. Peng, J. Weng, Widely-tunable, passively Q-switched erbium-doped fiber laser with few-layer MoS 2 saturable absorber, Opt. Express 22 (2014) 25258–25266.
[23] S. Wang, Y. Zhou, Y. Wang, S. Yan, Y. Li, W. Zheng, Y. Deng, Q. Zhu, J. Xu, Y. Tang, Digital-wavelength ytterbium fiber laser mode-locked with MoS2, Laser Phys. Lett. 13 (2016) 055102.
[24] H. Guoyu, Y. Song, K. Li, Z. Dou, J. Tian, X. Zhang, Mode-locked ytterbium-doped fiber laser based on tungsten disulphide, Laser Phys. Lett. 12 (2015) 125102.
[25] Z. Tian, K. Wu, L. Kong, N. Yang, Y. Wang, R. Chen, W. Hu, J. Xu, Y. Tang, Mode-locked thulium fiber laser with MoS2, Laser Phys. Lett. 12 (2015) 065104.
[26] B. Chen, X. Zhang, K. Wu, H. Wang, J. Wang, J. Chen, Q-switched fiber laser based on transition metal dichalcogenides MoS 2, MoSe 2, WS 2, and WSe 2, Opt. Express 23 (2015) 26723–26737.
[27] K. Wu, X. Zhang, J. Wang, X. Li, J. Chen, "Two-dimensional Nanomaterial Tungsten Disulfide (WS 2) As Saturable Absorber for Mode-locked Laser Near 1550 nm," in CLEO: Science and Innovations (Optical Society of America), p. JW2A. 66, 2015.
[28] K. Wu, X. Zhang, J. Wang, X. Li, J. Chen, WS 2 as a saturable absorber for ultrafast photonic applications of mode-locked and Q-switched lasers, Opt. Express 23 (2015) 11453–11461.
[29] E. Aharon, A. Albo, M. Kalina, G.L. Frey, Stable Blue Emission from a Polyfluorene/Layered-Compound Guest/Host Nanocomposite, Adv. Funct. Mater. 16 (2006) 980–986.
[30] Z. Zeng, Z. Yin, X. Huang, H. Li, Q. He, G. Lu, F. Boey, H. Zhang, Single-Layer Semiconducting Nanosheets: High-yield preparation and device fabrication, Angew. Chem. Int. Ed. 50 (2011) 11093–11097.
[31] H. Xia, H. Li, C. Lan, C. Li, X. Zhang, S. Zhang, Y. Liu, Ultrafast erbium-doped fiber laser mode-locked by a CVD-grown molybdenum disulfide (MoS 2) saturable absorber, Opt. Express 22 (2014) 17341–17348.
[32] P. Yan, R. Lin, S. Ruan, A. Liu, H. Chen, Y. Zheng, S. Chen, C. Guo, J. Hu, A practical topological insulator saturable absorber for mode-locked fiber laser, Sci. Rep. 5 (2015).
[33] J. Boguslawski, G. Sobon, R. Zybala, J. Sotor, Dissipative soliton generation in Er-doped fiber laser mode-locked by Sb 2 Te 3 topological insulator, Opt. Lett. 40 (2015) 2786–2789.
[34] M. Kowalczyk, J. Bogusławski, D. Stachowiak, J. Tarka, R. Zybala, K. Mars, A. Mikula, G.J. Sobon, J.Z. Sotor, K.M. Abramski, "All-normal dispersion Yb-doped fiber laser mode-locked by Sb2Te3 topological insulator," in SPIE Photonics Europe (International Society for Optics and Photonics), pp. 98930T-98930T-98937, 2016.

[35] B. Guo, Y. Yao, P.-G. Yan, K. Xu, J.-J. Liu, S.-G. Wang, Y. Li, Dual-Wavelength Soliton Mode-Locked Fiber Laser With a WS 2-Based Fiber Taper, IEEE Photonics Technol. Lett. 28 (2016) 323–326.
[36] H. Chen, I.L. Li, S. Ruan, T. Guo, P. Yan, Fiber-integrated tungsten disulfide saturable absorber (mirror) for pulsed fiber lasers, Opt. Eng. 55 (2016) (081318-081318).
[37] Z. Yi, W. Li, W. Jie Yu, L. Hong Wei, Y. Zhen Huang, Yb: yag thin disk laser passively Q-switched by a hydro-thermal grown molybdenum disulfide saturable absorber, Laser Phys. 25 (2015) 025901.
[38] S. Zhang, N. Dong, N. McEvoy, M. O'Brien, S. Winters, N.C. Berner, C. Yim, Y. Li, X. Zhang, Z. Chen, L. Zhang, G.S. Duesberg, J. Wang, Direct Observation of degenerate two-photon absorption and its saturation in WS2 and MoS2 monolayer and few-layer films, ACS Nano 9 (2015) 7142–7150.
[39] A. Castellanos-Gomez, M. Barkelid, A.M. Goossens, V.E. Calado, H.S.J. van der Zant, G.A. Steele, Laser-Thinning of MoS2: on Demand Generation of a Single-Layer Semiconductor, Nano Lett. 12 (2012) 3187–3192.
[40] B. Radisavljevic, A. Radenovic, J. Brivio, i.V. Giacometti, A. Kis, Single-layer MoS2 transistors, Nat. Nanotechnol. 6 (2011) 147–150.
[41] T. M, D.J. Late, Temperature dependent phonon shifts in single-layer WS2, ACS Appl. Mater. Interfaces 6 (2014) 1158–1163.
[42] C.-G. Andres, V. Leonardo, P. Elsa, O.I. Joshua, K.L. Narasimha-Acharya, I.B. Sofya, J.G. Dirk, B. Michele, A.S. Gary, J.V. Alvarez, W.Z. Henny, J.J. Palacios, S.J. v.d.Z. Herre, Isolation and characterization of few-layer black phosphorus, 2D Mater. 1 (2014) 025001.
[43] P. Tonndorf, R. Schmidt, P. Böttger, X. Zhang, J. Börner, A. Liebig, M. Albrecht, C. Kloc, O. Gordan, D.R.T. Zahn, S. Michaelis, de Vasconcellos, R. Bratschitsch, Photoluminescence emission and Raman response of monolayer MoS2, MoSe2, and WSe2, Opt. Express 21 (2013) 4908–4916.
[44] S. Zhang, J. Yang, R. Xu, F. Wang, W. Li, M. Ghufran, Y.-W. Zhang, Z. Yu, G. Zhang, Q. Qin, Y. Lu, Extraordinary Photoluminescence and Strong Temperature/Angle-Dependent Raman Responses in Few-Layer Phosphorene, ACS Nano 8 (2014) 9590–9596.
[45] G. Agrawal, "Chapter 2 - Pulse Propagation in Fibers," in Nonlinear Fiber Optics (Fifth Edition) (Academic Press), pp. 27–56, 2013.
[46] G. Wang, S. Zhang, X. Zhang, L. Zhang, Y. Cheng, D. Fox, H. Zhang, J.N. Coleman, W.J. Blau, J. Wang, Tunable nonlinear refractive index of two-dimensional MoS2, WS2, and MoSe2 nanosheet dispersions [Invited], Photonics Res. 3 (2015) A51–A55.
[47] R. Wu, Y. Zhang, S. Yan, F. Bian, W. Wang, X. Bai, X. Lu, J. Zhao, E. Wang, Purely Coherent Nonlinear Optical Response in Solution Dispersions of Graphene Sheets, Nano Lett. 11 (2011) 5159–5164.
[48] Q. Bao, H. Zhang, Y. Wang, Z. Ni, Y. Yan, Z.X. Shen, K.P. Loh, D.Y. Tang, Atomic-Layer Graphene as a Saturable Absorber for Ultrafast Pulsed Lasers, Adv. Funct. Mater. 19 (2009) 3077–3083.
[49] H. Zhang, S.B. Lu, J. Zheng, J. Du, S.C. Wen, D.Y. Tang, K.P. Loh, Molybdenum disulfide (MoS2) as a broadband saturable absorber for ultra-fast photonics, Opt. Express 22 (2014) 7249–7260.
[50] X. Liu, S. Guo, H. Wang, L. Hou, Theoretical study on the closed-aperture Z-scan curves in the materials with nonlinear refraction and strong nonlinear absorption, Opt. Commun. 197 (2001) 431–437.
[51] N. Dong, Y. Li, S. Zhang, N. McEvoy, X. Zhang, Y. Cui, L. Zhang, G.S. Duesberg, J. Wang, Dispersion of nonlinear refractive index in layered WS2 and WSe2 semiconductor films induced by two-photon absorption, Opt. Lett. 41 (2016) 3936–3939.
[52] B. Shi, L. Miao, Q. Wang, J. Du, P. Tang, J. Liu, C. Zhao, S. Wen, Broadband ultrafast spatial self-phase modulation for topological insulator Bi2Te3 dispersions, Appl. Phys. Lett. 107 (2015) 151101.
[53] J. Zhang, X. Yu, W. Han, B. Lv, X. Li, S. Xiao, Y. Gao, J. He, Broadband spatial self-phase modulation of black phosphorous, Opt. Lett. 41 (2016) 1704–1707.
[54] C. Wei, H. Luo, H. Zhang, C. Li, J. Xie, J. Li, Y. Liu, Passively Q-switched mid-infrared fluoride fiber laser around 3 μm using a tungsten disulfide (WS2) saturable absorber, Laser Phys. Lett. 13 (2016) 105108.
[55] J. Hou, G. Zhao, Y. Wu, J. He, X. Hao, Femtosecond solid-state laser based on tungsten disulfide saturable absorber, Opt. Express 23 (2015) 27292–27298.
[56] C. Guo, B. Chen, H. Wang, X. Zhang, J. Wang, K. Wu, J. Chen, Investigation on the stability of WSe2-PVA saturable absorber in an all PM Q-switched fiber laser, IEEE Photonics J. 8 (2016) 1–12.
[57] K. Wu, X. Zhang, J. Wang, J. Chen, 463-MHz fundamental mode-locked fiber laser based on few-layer MoS2 saturable absorber, Opt. Lett. 40 (2015) 1374–1377.
[58] Q. Wang, Y. Chen, L. Miao, G. Jiang, S. Chen, J. Liu, X. Fu, C. Zhao, H. Zhang, Wide spectral and wavelength-tunable dissipative soliton fiber laser with topological insulator nano-sheets self-assembly films sandwiched by PMMA polymer, Opt. Express 23 (2015) 7681–7693.
[59] P. Tang, M. Wu, Q. Wang, L. Miao, B. Huang, J. Liu, C. Zhao, S. Wen, 2.8-Pulsed Er 3+: ZBLAN fiber laser modulated by topological insulator, IEEE Photonics Technol. Lett. 28 (2016) 1573–1576.
[60] H. Wang, B. Chen, X. Zhang, S. Liu, B. Zhu, J. Wang, K. Wu, J. Chen, Ethanol catalytic deposition of MoS2 on tapered fiber, Photonics Res. 3 (2015) A102–A107.
[61] W. Liu, L. Pang, H. Han, W. Tian, H. Chen, M. Lei, P. Yan, Z. Wei, 70-fs mode-locked erbium-doped fiber laser with topological insulator, Sci. Rep. 5 (2016).
[62] P. Yan, R. Lin, H. Chen, H. Zhang, A. Liu, H. Yang, S. Ruan, Topological insulator solution filled in photonic crystal fiber for passive mode-locked fiber laser, IEEE Photonics Technol. Lett. 27 (2015) 264–267.
[63] B. Guo, Y. Yao, Y.-F. Yang, C. Liu, "Tunable multi-wavelength mode-locked fiber laser with topological insulator: Bi 2 Se 3/PVA solution," in Optoelectronic Devices and Integration (Optical Society of America), p. OW2C. 4, 2015.
[64] L. Gao, T. Zhu, W. Huang, Z. Luo, Stable, ultrafast pulse mode-locked by topological insulator nanosheets interacting with photonic crystal fiber: from anomalous dispersion to normal dispersion, IEEE Photonics J. 7 (2015) 1–8.
[65] K. Li, Y. Song, Z. Yu, J. Tian, "A 359fs Er-doped fiber laser based on topological insulator: Bi 2 Se 3," in Conference on Lasers and Electro-Optics/Pacific Rim (Optical Society of America), p. 26C21_23, 2015.
[66] B. Guo, Y. Yao, J.-J. Xiao, R.-L. Wang, J.-Y. Zhang, Topological insulator-assisted dual-wavelength fiber laser delivering versatile pulse patterns, IEEE J. Sel. Top. Quantum Electron. 22 (2016) 8–15.
[67] K. Li, Y. Song, Z. Yu, R. Xu, Z. Dou, J. Tian, L-band femtosecond fibre laser based on Bi2Se3 topological insulator, Laser Phys. Lett. 12 (2015) 105103.
[68] G. Semaan, Y. Meng, M. Salhi, A. Niang, K. Guesmi, Z.-C. Luo, F. Sanchez, "High power passive mode-locked L-band fiber laser based on microfiber topological insulator saturable absorber," in SPIE Photonics Europe (International Society for Optics and Photonics), pp. 98930R-98930R-98937, 2016.
[69] C. Chi, J. Lee, J. Koo, J.H. Lee, All-normal-dispersion dissipative-soliton fiber laser at 1.06 μm using a bulk-structured Bi2Te3 topological insulator-deposited side-polished fiber, Laser Phys. 24 (2014) 105106.
[70] J. Boguslawski, J. Sotor, G. Sobon, R. Zybala, M. Kowalczyk, J. Tarka, D. Sliwinska, K. Abramski, "Sub-200 fs dissipative soliton Er-doped fiber laser mode-locked by Sb 2 Te 3 topological insulator," in The European Conference on Lasers and Electro-Optics (Optical Society of America), p. CF_P_5, 2015.
[71] J. Lee, J. Koo, Y.M. Jhon, J.H. Lee, Femtosecond harmonic mode-locking of a fiber laser based on a bulk-structured Bi 2 Te 3 topological insulator, Opt. Express 23 (2015) 6359–6369.
[72] P. Yan, R. Lin, S. Ruan, A. Liu, H. Chen, A 2.95 GHz, femtosecond passive harmonic mode-locked fiber laser based on evanescent field interaction with topological insulator film, Opt. Express 23 (2015) 154–164.
[73] K. Yin, B. Zhang, L. Li, T. Jiang, X. Zhou, J. Hou, Soliton mode-locked fiber laser based on topological insulator Bi 2 Te 3 nanosheets at 2 μm, Photonics Res. 3 (2015) 72–76.
[74] M. Jung, J. Lee, J. Koo, J. Park, Y.-W. Song, K. Lee, S. Lee, J.H. Lee, A femtosecond pulse fiber laser at 1935 nm using a bulk-structured Bi 2 Te 3 topological insulator, Opt. Express 22 (2014) 7865–7874.
[75] S. Sathiyan, V. Velmurugan, K. Senthilnathan, P. Ramesh Babu, S. Sivabalan, All-normal dispersion passively mode-locked Yb-doped fiber laser using MoS2–PVA saturable absorber, Laser Phys. 26 (2016) 055103.
[76] Y. Zhan, C. Wang, Nanosecond pulse generation in a MoS2 mode-locked ytterbium-doped fiber laser, Opt. Quantum Electron. 48 (2016).
[77] C. Feng, X. Zhang, J. Wang, Z. Liu, Z. Cong, H. Rao, Q. Wang, J. Fang, Passively mode-locked Nd^3+: yvo_4 laser using a molybdenum disulfide as saturable absorber, Opt. Mater. Express 6 (2016) 1358.
[78] Y. Wang, D. Mao, X. Gan, L. Han, C. Ma, T. Xi, Y. Zhang, W. Shang, S. Hua, J. Zhao, Harmonic mode locking of bound-state solitons fiber laser based on MoS(2) saturable absorber, Opt. Express 23 (2015) 205–210.
[79] R.C.T. Howe, R.I. Woodward, G. Hu, Z. Yang, E.J.R. Kelleher, T. Hasan, Surfactant-aided exfoliation of molybdenum disulfide for ultrafast pulse generation through edge-state saturable absorption, Physica Status Solidi (b) 253 (2016) 911–917.
[80] M. Liu, X.W. Zheng, Y.L. Qi, H. Liu, A.P. Luo, Z.C. Luo, W.C. Xu, C.J. Zhao, H. Zhang, Microfiber-based few-layer MoS2 saturable absorber for 2.5 GHz passively harmonic mode-locked fiber laser, Opt. Express 22 (2014) 22841–22846.
[81] A.-P. Luo, M. Liu, X.-D. Wang, Q.-Y. Ning, W.-C. Xu, Z.-C. Luo, Few-layer MoS2-deposited microfiber as highly nonlinear photonic device for pulse shaping in a fiber laser [Invited], Photonics Res. 3 (2015) A69–A78.
[82] D. Li-Na, S. Yu-Long, W. Yong-Gang, L. Lu, W. Xi, W. Yi-Shan, Passively mode-locked erbium-doped fiber laser via a D-shape-fiber-based MoS 2 saturable absorber with a very low nonsaturable loss, Chin. Phys. B 25 (2016) 024206.
[83] R. Khazaeizhad, S.H. Kassani, H. Jeong, D.I. Yeom, K. Oh, Mode-locking of Er-doped fiber laser using a multilayer MoS2 thin film as a saturable absorber in both anomalous and normal dispersion regimes, Opt. Express 22 (2014) 23732–23742.
[84] S. Srivastava, B. Avasthi, Layer type tungsten dichalcogenide compounds: their preparation, structure, properties and uses, J. Mater. Sci. 20 (1985) 3801–3815.
[85] L. Li, S. Jiang, Y. Wang, X. Wang, L. Duan, D. Mao, Z. Li, B. Man, J. Si, WS(2)/fluorine mica (FM) saturable absorbers for all-normal-dispersion mode-locked fiber laser, Opt. Express 23 (2015) 28698–28706.

[86] W. Liu, L. Pang, H. Han, Z. Shen, M. Lei, H. Teng, Z. Wei, Dark solitons in WS_2 erbium-doped fiber lasers, Photonics Res. 4 (2016) 111.

[87] P. Yan, H. Chen, A. Liu, K. Li, S. Ruan, J. Ding, X. Qiu, T. Guo, Self-starting mode-locking by fiber-integrated WS2 saturable absorber mirror, IEEE J. Sel. Top. Quantum Electron. 23 (2017) 1–6.

[88] L. Li, Y. Su, Y. Wang, X. Wang, Y. Wang, X. Li, D. Mao, J. Si, Femtosecond passively Er-doped mode-locked fiber laser With WS2 solution saturable absorber, IEEE J. Sel. Top. Quantum Electron. 23 (2016) 1–6.

[89] D. Mao, Y. Wang, C. Ma, L. Han, B. Jiang, X. Gan, S. Hua, W. Zhang, T. Mei, J. Zhao, WS2 mode-locked ultrafast fiber laser, Sci. Rep. 5 (2015) 7965.

[90] J. Lee, J. Park, J. Koo, Y.M. Jhon, J.H. Lee, Harmonically mode-locked femtosecond fiber laser using non-uniform, WS2-particle deposited side-polished fiber, J. Opt. 18 (2016) 035502.

[91] R. Khazaeinezhad, S.H. Kassani, H. Jeong, K.J. Park, B.Y. Kim, D.I. Yeom, K. Oh, Ultrafast pulsed all-fiber laser based on tapered fiber enclosed by few-layer WS2 nanosheets, IEEE Photonics Technol. Lett. 27 (2015) 1581–1584.

[92] B. Guo, Q. Lyu, Y. Yao, P. Wang, Direct generation of dip-type sidebands from WS_2 mode-locked fiber laser, Opt. Mater. Express 6 (2016) 2475.

[93] D.-P. Zhou, L. Wei, B. Dong, W.-K. Liu, Tunable passively-switched erbium-doped fiber laser with carbon nanotubes as a saturable absorber, Photonics Technol. Lett., IEEE 22 (2010) 9–11.

[94] M. Jung, J. Lee, J. Park, J. Koo, Y.M. Jhon, J.H. Lee, Mode-locked, 1.94-mum, all-fiberized laser using WS(2) based evanescent field interaction, Opt. Express 23 (2015) 19996–20006.

[95] D. Mao, X. She, B. Du, D. Yang, W. Zhang, K. Song, X. Cui, B. Jiang, T. Peng, J. Zhao, Erbium-doped fiber laser passively mode locked with few-layer WSe2/MoSe2 nanosheets, Sci. Rep. 6 (2016) 23583.

[96] J. Koo, J. Park, J. Lee, Y.M. Jhon, J.H. Lee, Femtosecond harmonic mode-locking of a fiber laser at 3.27 GHz using a bulk-like, MoSe2-based saturable absorber, Opt. Express 24 (2016) 10575–10589.

[97] Z. Luo, Y. Li, M. Zhong, Y. Huang, X. Wan, J. Peng, J. Weng, Nonlinear optical absorption of few-layer molybdenum diselenide (MoSe2) for passively mode-locked soliton fiber laser [Invited], Photonics Res. 3 (2015) A79–A86.

[98] D. Mao, B. Du, D. Yang, S. Zhang, Y. Wang, W. Zhang, X. She, H. Cheng, H. Zeng, J. Zhao, Nonlinear Saturable Absorption of Liquid-Exfoliated Molybdenum/Tungsten Ditelluride Nanosheets, Small (2016).

[99] J. Koo, Y.I. Jhon, J. Park, J. Lee, Y.M. Jhon, J.H. Lee, Near-infrared saturable absorption of defective bulk-structured WTe2 for femtosecond laser mode-locking, Adv. Funct. Mater. 26 (2016) 7454–7461.

[100] X. Su, Y. Wang, B. Zhang, R. Zhao, K. Yang, J. He, Q. Hu, Z. Jia, X. Tao, Femtosecond solid-state laser based on a few-layered black phosphorus saturable absorber, Opt. Lett. 41 (2016) 1945–1948.

[101] B. Zhang, F. Lou, R. Zhao, J. He, J. Li, X. Su, J. Ning, K. Yang, Exfoliated layers of black phosphorus as saturable absorber for ultrafast solid-state laser, Opt. Lett. 40 (2015) 3691–3694.

[102] M. Hisyam, M. Rusdi, A. Latiff, S. Harun, "Generation of Mode-locked Ytterbium doped fiber ring laser using few-layer black phosphorus as a saturable absorber.".

[103] S. Zhang, X. Zhang, H. Wang, B. Chen, K. Wu, K. Wang, D. Hanlon, J.N. Coleman, J. Chen, L. Zhang, Size-dependent saturable absorption and mode-locking of dispersed black phosphorus nanosheets, Opt. Mater. Express 6 (2016) 3159–3168.

[104] K. Park, J. Lee, Y.T. Lee, W.K. Choi, J.H. Lee, Y.W. Song, Black phosphorus saturable absorber for ultrafast mode-locked pulse laser via evanescent field interaction, Ann. der Phys. 527 (2015) 770–776.

[105] D. Li, H. Jussila, L. Karvonen, G. Ye, H. Lipsanen, X. Chen, Z. Sun, Polarization and thickness dependent absorption properties of black phosphorus: new saturable absorber for ultrafast pulse generation, Sci. Rep. 5 (2015).

[106] D. Li, H. Jussila, L. Karvonen, G. Ye, H. Lipsanen, X. Chen, Z. Sun, Ultrafast pulse generation with black phosphorus, arXiv Prepr. arXiv 1505 (2015) 00480.

[107] Y. Song, S. Chen, Q. Zhang, L. Li, L. Zhao, H. Zhang, D. Tang, Vector soliton fiber laser passively mode locked by few layer black phosphorus-based optical saturable absorber, Opt. Express 24 (2016) 25933–25942.

[108] J. Sotor, G. Sobon, W. Macherzynski, P. Paletko, K.M. Abramski, Black phosphorus saturable absorber for ultrashort pulse generation, Appl. Phys. Lett. 107 (2015) 051108.

[109] M. Ahmed, A. Latiff, H. Arof, S. Harun, Ultrafast erbium-doped fiber laser mode-locked with a black phosphorus saturable absorber, Laser Phys. Lett. 13 (2016) 095104.

[110] Z.-C. Luo, M. Liu, Z.-N. Guo, X.-F. Jiang, A.-P. Luo, C.-J. Zhao, X.-F. Yu, W.-C. Xu, H. Zhang, Microfiber-based few-layer black phosphorus saturable absorber for ultra-fast fiber laser, Opt. Express 23 (2015) 20030–20039.

[111] Y. Chen, H. Mu, P. Li, S. Lin, B.N. Shivananju, Q. Bao, Optically driven black phosphorus as a saturable absorber for mode-locked laser pulse generation, Opt. Eng. 55 (2016) (081317-081317).

[112] Y. Chen, S. Chen, J. Liu, Y. Gao, W. Zhang, Sub-300 femtosecond soliton tunable fiber laser with all-anomalous dispersion passively mode locked by black phosphorus, Opt. Express 24 (2016) 13316–13324.

[113] H. Yu, X. Zheng, K. Yin, T. Jiang, Thulium/holmium-doped fiber laser passively mode locked by black phosphorus nanoplatelets-based saturable absorber, Appl. Opt. 54 (2015) 10290–10294.

[114] J. Sotor, G. Sobon, M. Kowalczyk, W. Macherzynski, P. Paletko, K.M. Abramski, Ultrafast thulium-doped fiber laser mode locked with black phosphorus, Opt. Lett. 40 (2015) 3885–3888.

[115] Z. Qin, G. Xie, C. Zhao, S. Wen, P. Yuan, L. Qian, Mid-infrared mode-locked pulse generation with multilayer black phosphorus as saturable absorber, Opt. Lett. 41 (2016) 56–59.

[116] J. Li, H. Luo, B. Zhai, R. Lu, Z. Guo, H. Zhang, Y. Liu, Black phosphorus: a two-dimension saturable absorption material for mid-infrared Q-switched and mode-locked fiber lasers, Sci. Rep. 6 (2016).

[117] H. Zhang, C.-X. Liu, X.-L. Qi, X. Dai, Z. Fang, S.-C. Zhang, Topological insulators in Bi2Se3, Bi2Te3 and Sb2Te3 with a single Dirac cone on the surface, Nat. Phys. 5 (2009) 438–442.

[118] Y. Chen, J. Analytis, J.-H. Chu, Z. Liu, S.-K. Mo, X.-L. Qi, H. Zhang, D. Lu, X. Dai, Z. Fang, Experimental realization of a three-dimensional topological insulator, Bi2Te3, Science 325 (2009) 178–181.

[119] R. Woodward, E. Kelleher, R. Howe, G. Hu, F. Torrisi, T. Hasan, S. Popov, J. Taylor, Tunable Q-switched fiber laser based on saturable edge-state absorption in few-layer molybdenum disulfide (MoS 2), Opt. Express 22 (2014) 31113–31122.

[120] S.H. Kassani, R. Khazaeinezhad, H. Jeong, T. Nazari, D.-I. Yeom, K. Oh, All-fiber Er-doped Q-Switched laser based on Tungsten Disulfide saturable absorber, Opt. Mater. Express 5 (2015) 373–379.

[121] V. Tran, R. Soklaski, Y. Liang, L. Yang, Layer-controlled band gap and anisotropic excitons in few-layer black phosphorus, Phys. Rev. B 89 (2014) 235319.

[122] C. Hönninger, R. Paschotta, F. Morier-Genoud, M. Moser, U. Keller, Q-switching stability limits of continuous-wave passive mode locking, J. Opt. Soc. Am. B 16 (1999) 46–56.

[123] D. Wu, Z. Cai, Y. Zhong, J. Peng, J. Weng, Z. Luo, N. Chen, H. Xu, 635-nm visible Pr3-doped ZBLAN fiber lasers Q-switched by topological insulators SAs, IEEE Photonics Technol. Lett. 27 (2015) 2379–2382.

[124] B. Xu, Y. Wang, J. Peng, Z. Luo, H. Xu, Z. Cai, J. Weng, Topological insulator Bi 2 Se 3 based Q-switched Nd: LiYF 4 ns laser at 1313 nm, Opt. Express 23 (2015) 7674–7680.

[125] S. Chen, Y. Chen, M. Wu, Y. Li, C. Zhao, S. Wen, Stable-switched erbium-doped fiber laser based on topological insulator covered Microfiber, IEEE Photonics Technol. Lett. 26 (2014) 987–990.

[126] Y. Chen, C. Zhao, H. Huang, S. Chen, P. Tang, Z. Wang, S. Lu, H. Zhang, S. Wen, D. Tang, Self-Assembled Topological Insulator: Bi Se Membrane as a Passive Q-Switcher in an Erbium-Doped Fiber Laser, J. Light. Technol. 31 (2013) 2857–2863.

[127] P. Tang, X. Zhang, C. Zhao, Y. Wang, H. Zhang, D. Shen, S. Wen, D. Tang, D. Fan, Topological insulator: saturable absorber for the passive Q-switching operation of an in-band pumped 1645-nm Er: YAG ceramic laser, IEEE Photonics J. 5 (2013) (1500707-1500707).

[128] J. Lee, M. Jung, J. Koo, C. Chi, J.H. Lee, Passively Q-switched 1.89-μm fiber laser using a bulk-structured Bi 2 Te 3 topological insulator, IEEE J. Sel. Top. Quantum Electron. 21 (2015) 31–36.

[129] Z. Luo, C. Liu, Y. Huang, D. Wu, J. Wu, H. Xu, Z. Cai, Z. Lin, L. Sun, J. Weng, Topological-insulator passively Q-switched double-clad fiber laser at 2 m wavelength, IEEE J. Sel. Top. Quantum Electron. 20 (2014) 1–8.

[130] J. Lee, J. Koo, C. Chi, J.H. Lee, All-fiberized, passively Q-switched 1.06 μm laser using a bulk-structured Bi2Te3 topological insulator, J. Opt. 16 (2014) 085203.

[131] W. Li, J. Peng, Y. Zhong, D. Wu, H. Lin, Y. Cheng, Z. Luo, J. Weng, H. Xu, Z. Cai, Orange-light passively Q-switched Pr3+-doped all-fiber lasers with transition-metal dichalcogenide saturable absorbers, Opt. Mater. Express 6 (2016) 2031–2039.

[132] Z. Luo, D. Wu, B. Xu, H. Xu, Z. Cai, J. Peng, J. Weng, S. Xu, C. Zhu, F. Wang, Two-dimensional material-based saturable absorbers: towards compact visible-wavelength all-fiber pulsed lasers, Nanoscale 8 (2016) 1066–1072.

[133] P. Li, B. Liang, M. Su, Y. Zhang, Y. Zhao, M. Zhang, C. Ma, N. Su, 980-nm Q-switched photonic crystal fiber laser by MoS2 saturable absorber, Appl. Phys. B 122 (2016).

[134] Z. Luo, Y. Huang, M. Zhong, Y. Li, J. Wu, B. Xu, H. Xu, Z. Cai, J. Peng, J. Weng, 1-, 1.5-, and 2-μm fiber lasers Q-switched by a broadband few-layer MoS 2 saturable absorber, J. Light. Technol. 32 (2014) 4077–4084.

[135] F. Zhang, X. Li, H. Zhang, T. Chen, C. Zhou, "Passively Q-switched Nd:YVO <inf>4</inf>laser by MoS<inf>2</inf>with 164ns pulse width," in 2016 IEEE MTT-S International Microwave Workshop Series on Advanced Materials and Processes for RF and THz Applications (IMWS-AMP), pp. 1–4, 2016.

[136] R.I. Woodward, E.J. Kelleher, T. Runcorn, S.V. Popov, F. Torrisi, R.T. Howe, T. Hasan, Q-switched fiber laser with MoS2 saturable absorber, CLEO: 2014, SM3H-6 (2014).

[137] J. Ren, S. Wang, Z. Cheng, H. Yu, H. Zhang, Y. Chen, L. Mei, P. Wang, Passively Q-switched nanosecond erbium-doped fiber laser with MoS(2) saturable absorber, Opt. Express 23 (2015) 5607–5613.

[138] P. Ge, J. Liu, S. Jiang, Y. Xu, B. Man, Compact Q-switched 2 μm Tm:GdVO4 laser with MoS2 absorber, Photonics Res. 3 (2015) 256–259.

[139] S. Wang, H. Yu, H. Zhang, A. Wang, M. Zhao, Y. Chen, L. Mei, J. Wang, Broadband few-layer MoS2 saturable absorbers, Adv. Mater. 26 (2014) 3538–3544.

[140] Z. Luo, M. Zhou, J. Weng, G. Huang, H. Xu, C. Ye, Z. Cai, Graphene-based passively Q-switched dual-wavelength erbium-doped fiber laser, Opt. Lett. 35 (2010) 3709–3711.

[141] M. Zhang, G. Hu, G. Hu, R.C. Howe, L. Chen, Z. Zheng, T. Hasan, Yb- and Er-doped fiber laser Q-switched with an optically uniform, broadband WS2 saturable absorber, Sci. Rep. 5 (2015) 17482.
[142] J. Lin, Y. Hu, C. Chen, C. Gu, L. Xu, Wavelength-tunable Yb-doped passively Q-switching fiber laser based on WS(2) saturable absorber, Opt. Express 23 (2015) 29059–29064.
[143] X. Wang, Y. Wang, L. Duan, L. Li, H. Sun, Passively Q-switched nd:YAG laser via a WS2 saturable absorber, Opt. Commun. 367 (2016) 234–238.
[144] H. Chen, Y. Chen, J. Yin, X. Zhang, T. Guo, P. Yan, High-damage-resistant tungsten disulfide saturable absorber mirror for passively Q-switched fiber laser, Opt. Express 24 (2016) 16287–16296.
[145] H. Ahmad, N.E. Ruslan, M.A. Ismail, S.A. Reduan, C.S. Lee, S. Sathiyan, S. Sivabalan, S.W. Harun, Passively Q-switched erbium-doped fiber laser at C-band region based on WS(2) saturable absorber, Appl. Opt. 55 (2016) 1001–1005.
[146] C. Bohua, W. Hao, X. Zhang, J. Wang, K. Wu, J. Chen, "Q-switched ring-cavity erbium-doped fiber laser based on tungsten disulfide (WS2)," in Opto-Electronics and Communications Conference (OECC), 201, 5, 2015, pp. 1–3.
[147] R. Khazaeinezhad, T. Nazari, H. Jeong, K.J. Park, B.Y. Kim, D.-I. Yeom, K. Oh, Passive Q-Switching of an All-Fiber Laser Using WS 2-Deposited Optical Fiber Taper, IEEE Photonics J. 7 (2015) 1–7.
[148] C. Cheng, H. Liu, Y. Tan, J.R. Vazquez de Aldana, F. Chen, Passively Q-switched waveguide lasers based on two-dimensional transition metal diselenide, Opt. Express 24 (2016) 10385–10390.
[149] B. Chen, X. Zhang, C. Guo, K. Wu, J. Chen, J. Wang, Tungsten diselenide Q-switched erbium-doped fiber laser, Opt. Eng. 55 (2016) 081306.
[150] R.I. Woodward, R.C. Howe, T.H. Runcorn, G. Hu, F. Torrisi, E.J. Kelleher, T. Hasan, Wideband saturable absorption in few-layer molybdenum diselenide (MoSe(2)) for Q-switching Yb-, Er- and Tm-doped fiber lasers, Opt. Express 23 (2015) 20051–20061.
[151] H. Ahmad, M. Suthaskumar, Z.C. Tiu, A. Zarei, S.W. Harun, Q-switched erbium-doped fiber laser using MoSe2 as saturable absorber, Opt. Laser Technol. 79 (2016) 20–23.
[152] D. Wu, Z. Cai, Y. Zhong, J. Peng, Y. Cheng, J. Weng, Z. Luo, H. Xu, "Compact passive Q-switching Pr3+-doped ZBLAN fiber laser with black phosphorus-based saturable absorber".
[153] L. Kong, Z. Qin, G. Xie, Z. Guo, H. Zhang, P. Yuan, L. Qian, Black phosphorus as broadband saturable absorber for pulsed lasers from 1 μm to 2.7 μm wavelength, Laser Phys. Lett. 13 (2016) 045801.
[154] F. Rashid, S.R. Azzuhri, M. Salim, R. Shaharuddin, M. Ismail, M. Ismail, M. Razak, H. Ahmad, Using a black phosphorus saturable absorber to generate dual wavelengths in a Q-switched ytterbium-doped fiber laser, Laser Phys. Lett. 13 (2016) 085102.
[155] J. Ma, S. Lu, Z. Guo, X. Xu, H. Zhang, D. Tang, D. Fan, Few-layer black phosphorus based saturable absorber mirror for pulsed solid-state lasers, Opt. Express 23 (2015) 22643–22648.
[156] H. Ahmad, M. Salim, K. Thambiratnam, S. Norizan, S. Harun, A black phosphorus-based tunable Q-switched ytterbium fiber laser, Laser Phys. Lett. 13 (2016) 095103.
[157] R. Zhang, Y. Zhang, H. Yu, H. Zhang, R. Yang, B. Yang, Z. Liu, J. Wang, Broadband Black Phosphorus Optical Modulator in the Spectral Range from Visible to Mid-Infrared, Adv. Opt. Mater. 3 (2015) 1787–1792.
[158] A. Al-Masoodi, M. Ahmed, A. Latiff, H. Arof, S. Harun, Q-Switched Ytterbium-Doped Fiber Laser Using Black Phosphorus as Saturable Absorber, Chin. Phys. Lett. 33 (2016) 054206.
[159] T. Jiang, K. Yin, X. Zheng, H. Yu, X.-A. Cheng, Black phosphorus as a new broadband saturable absorber for infrared passively Q-switched fiber lasers, arXiv Prepr. arXiv 1504 (2015) 07341.
[160] T. Feng, D. Mao, X. Cui, M. Li, K. Song, B. Jiang, H. Lu, W. Quan, A Filmy black-phosphorus polyimide saturable absorber for Q-switched operation in an erbium-doped fiber laser, Materials 9 (2016) 917.
[161] H. Mu, S. Lin, Z. Wang, S. Xiao, P. Li, Y. Chen, H. Zhang, H. Bao, S.P. Lau, C. Pan, Black phosphorus–polymer composites for pulsed lasers, Adv. Opt. Mater. 3 (2015) 1447–1453.
[162] H. Yu, X. Zheng, K. Yin, T. Jiang, Nanosecond passively Q-switched thulium/holmium-doped fiber laser based on black phosphorus nanoplatelets, Opt. Mater. Express 6 (2016) 603–609.
[163] H. Zhang, J. He, Z. Wang, J. Hou, B. Zhang, R. Zhao, K. Han, K. Yang, H. Nie, X. Sun, Dual-wavelength, passively Q-switched Tm: YAP laser with black phosphorus saturable absorber, Opt. Mater. Express 6 (2016) 2328–2335.
[164] Z. Chu, J. Liu, Z. Guo, H. Zhang, 2 μm passively Q-switched laser based on black phosphorus, Opt. Mater. Express 6 (2016) 2374–2379.
[165] Y. Xie, L. Kong, Z. Qin, G. Xie, J. Zhang, Black phosphorus-based saturable absorber for Q-switched Tm: yag ceramic laser, Opt. Eng. 55 (2016) (081307-081307).
[166] Z. Wang, R. Zhao, J. He, B. Zhang, J. Ning, Y. Wang, X. Su, J. Hou, F. Lou, K. Yang, Multi-layered black phosphorus as saturable absorber for pulsed Cr: ZnSe laser at 2.4 μm, Opt. Express 24 (2016) 1598–1603.
[167] Z. Qin, G. Xie, H. Zhang, C. Zhao, P. Yuan, S. Wen, L. Qian, Black phosphorus as saturable absorber for the Q-switched Er: ZBLAN fiber laser at 2.8 μm, Opt. Express 23 (2015) 24713–24718.
[168] K. Wu, X. Li, Y. Wang, Q.J. Wang, P.P. Shum, J. Chen, Towards low timing phase noise operation in fiber lasers mode locked by graphene oxide and carbon nanotubes at 1.5 μm, Opt. Express 23 (2015) 501–511.
[169] B. Huang, J. Yi, L. Du, G. Jiang, L. Miao, P. Tang, J. Liu, Y. Zou, H. Luo, C. Zhao, S. Wen, Graphene Q-Switched Vectorial Fiber Laser With Switchable Polarized Output, IEEE J. Sel. Top. Quantum Electron. 23 (2017) 1–7.